First of all we would like to thank the reviewer for very detailed comments and useful suggestions, which helped us to improve the revised manuscript

The manuscript describes several case studies of lidar observations where fluorescence observations combined with lidar depolarization shows significantly different properties for pollen, smoke, dust and anthropogenic aerosol. I'm excited to see the potential of these new measurements, which give completely independent and orthogonal information about aerosol particles, at single bin resolutions, significantly increasing the information available for aerosol typing. The case studies are a nice selection of different types and mixtures and interesting to see.

The manuscript seems to suffer from an identity problem, however. Mostly it is an illustrative set of cases studies that demonstrate differences in the two-dimensional space of fluorescence capacity and particle depolarization. It includes nice analysis of some mixtures of types as well. However, the paper claims to be an algorithm description paper, and for that purpose, analysis of a few hand-selected case studies really isn't sufficient, and the mixture analysis doesn't exactly fit, because it is not part of the algorithm. Apparently in consequence of this uncertainty about the desired focus of the paper, some aspects of the paper seem superficial, or rather, inconsistent in depth. The inferences in the paper about the types seem very reasonable, but many are not backed up by any independent information or compared with other methods of classification, which should be done to demonstrate the validity of the new algorithm, particularly if this is the algorithm description paper. Also there's insufficient information about how the thresholds in the algorithm were chosen. In the analysis of the case studies, there should be a consistent effort to include complimentary information to validate the case identifications using other measurements (in situ or other lidar measurements that reveal type) and backtrajectories. And if a major focus of the paper is to showcase the performance of a new (and better) classification algorithm, then the results should be shown on a bulk of data in addition to the case studies, and comparisons with other classification methods should be made and discussed.

The goal of this manuscript is to demonstrate that the fluorescence – depolarization diagram allows to separate different types of aerosol and provides new independent information on aerosol type, which can be used in classification schemes. The reviewer is right, at current stage of research it is not appropriate to call it “algorithm”, so we escape this term in the revised manuscript.
In the revised manuscript we tried to follow the reviewer recommendations. We added a table, containing the particle intensive parameters for the cases considered (lidar ratios at 355 and 532 nm; depolarization ratios at 355, 532 and 1064 nm; and the backscattering and extinction Angstrom exponents). Another table provides the range of variation of particle intensive properties from different typing algorithms for the urban, smoke and dust particles. The table contains also the range of parameters variation for episodes from current study for the same aerosol types.
The back-trajectory analysis is included.
In Appendix we added four maps with SILAM pollen index, for the episodes where the presence of the pollen was revealed. We hope, that all this improved the manuscript.

Specific comments:

L24. "and their mixtures". The mixture analysis is an interesting part of the paper, and apparently new compared to the authors' other papers, but it appears it's not really part of the classification algorithm, in the sense that mixture analysis can only be done on a case-by-case basis. Any discussion about that? This could be clarified in the abstract. Also, the mixture analysis is not even mentioned in the introduction. Discussing it there would help to clarify the novel aspects of the paper.

The mixture analysis is an important but in the manuscript presented we just identify the main mixture components, based on the patterns in depolarization – fluorescence diagram. Quantification of the mixture composition is the next step in our research and corresponding algorithm is in preparation at the moment. We removed from Abstract the mentioning of mixture analysis.

L73-75. I very much agree that adding independent aerosol information will improve classification, but this specific point is unconvincing. Yes, the variables used for classification so far have variability within types but there's nothing to suggest that this won't also be true for fluorescence capacity, is there? So, I'm not sure this is exactly the right motivation.

The advantage of fluorescence is strong variation of fluorescence capacity between some aerosol types. For example, G_F of smoke can up to one order higher, comparing to urban aerosol, allowing to separate these particles. So we think, that synergy of existing algorithms with fluorescence measurements should improve identification. Another important advantage is that G_F and depolarization can be derived with high spatio – temporal resolution, so almost single pixel typing becomes possible.

L105. Good point that the resolution is higher since fluorescence capacity can be calculated using data at a single bin, unlike extinction or other quantities related to extinction. This seems particularly useful for Raman measurements.

Yes.

L105-107. Veselovskii et al. 2021a is referenced extensively in the introduction, including to say that it already demonstrates the ability of the 2-d measurement space to separate all the aerosol types. I couldn't follow how the purpose and scope of this paper is different from 2021a.

In that paper we just formulated the idea and plotted averaged data for several observations on the depolarization – fluorescence diagram. In this manuscript we evaluate the aerosol type mask with almost singe pixel resolution. Corresponding paragraph is added to the revised manuscript.

L183-193. Calculation of the backscatter coefficient using a calibration constant sounds so straightforward, that I didn't realize that it hadn't been done before. This is great. It's good to see a relatively straightforward innovation discovered and put into practice that will produce a significant amount of additional retrievals, in profiles when the reference height is not accessible to the lidar.

We are very pleased, that Reviewer liked our approach

L231-232. Add an earlier reference for spectral dependence of the depolarization ratio, Burton et al. 2015.
Added

L240-241. Since line 223 just said that Veselovskii et al. 2021a already demonstrated that the two dimensional diagram can separate types, is the part about mixtures the main purpose of this manuscript? If so, the abstract and intro should make that clearer and the examples should be chosen to align with that purpose.

We modified Introduction, to show that the main goal is to provide aerosol type mask with high spatio-temporal resolution. The patterns at δ_{532}-G_F diagram help to identify the mixture, but at current stage we can not characterize it quantitatively.

L248-249. Burton et al. (2012) or Burton et al. (2013), referenced elsewhere in the manuscript, is an earlier lidar aerosol classification methodology with depolarization ratio ranges listed for common types.

Added

L247. "The ranges are based on results obtained in LOA". The algorithm is a simple thresholding method in two dimensions, so the ranges are the single most important aspect of the algorithm description. This statement is much too vague to support and explain how the ranges were derived, and I'm eager to know more. What results? From cases published in other publications? From a completely independent subset of cases than the results shown in this manuscript? Are the results only inferences from the lidar measurements of depolarization and fluorescence capacity, or do they include other coincident measurements that provide stronger evidence for the type identifications? Is there a set of training cases that are classified using other external measurements and/or source information? Are the cases shown in this paper the training cases or are they independent cases that demonstrate the validation of the algorithm? All this should be part of the methodology discussion.

We agree with reviewer and completely modified that section. We added:

"**Dust**. The depolarization ratio δ_{532} of Saharan dust near the source regions is up to 35% (Veselovskii et al., 2020a), but after transportation and mixing with local aerosol δ_{532} can be as low as 20% (Rittmeister et al., 2017). In many studies, the dust with decreased depolarization ratio is classified as "polluted dust" (e.g. Burton et al., 2012, 2013). At a moment, we do not introduce the discrimination between the two subtypes and mark as "dust" the particles with 20%<δ_{532}<35%, and $0.1\times10^{-4}<G_F<0.5\times10^{-4}$.

Smoke. In 2021-2022 we regular observed over Lille the smoke layers originated from Californian and Canadian forest fires (Hu et al., 2021). The particle depolarization and fluorescence capacity of transported smoke changed from episode to episode and for classification we choose the ranges 2%<δ_{532}<10%, $2\times10^{-4}<G_F<6\times10^{-4}$. At this stage we do not discriminate "fresh" and "aged" smoke, and the range of δ_{532} variation is similar to the one, used in classification of Burton et al. (2012).

Pollen. The pollen over north of France is usually mixed with other aerosols, and the particles, which we mark as "pollen" are actually the mixtures. Depolarization ratio of clean pollen varies strongly for different taxa. For birch pollen, Cao et al. (2010) reported δ_{532}=33%, and in the measurements over Finland during birch pollination (Bohlmann et al., 2019), observed values of δ_{532} up to 26%. The observations over Lille during pollen season (Veselovskii et al., 2021a) rarely revealed values δ_{532} exceeding 20%. Based on that observations, we type as "pollen" the particles mixtures with 15%<δ_{532}<30%, and $0.8\times10^{-4}<G_F<3.0\times10^{-4}$.

Urban. This type of aerosol includes a variety of particle types (e.g. sulfates, soot) and its parameters may depend on the relative humidity. Based on our measurements inside the boundary layer, for classification we choose the ranges 1%<δ_{532}<8%, and $0.1\times10^{-4}<G_F<0.8\times10^{-}$

[4]. Similar range for δ_{532} is used in classification of Burton et al. (2012). Urban and smoke particles both have a low depolarization, but the fluorescence capacity of smoke is almost one order higher, so these particles can be reliably discriminated.

Ice and water clouds. Both types of the clouds have low fluorescence capacity G_F $<0.01\times10^{-4}$. However, the ice clouds are usually observed at the heights, where fluorescence signal is low and can not be used for classification. Thus above ~8 km the ice cloud are identified by high depolarization ratio δ_{532}>40%. Depolarization ratio of the liquid water clouds is usually affected by the effects of the multiple scattering, so for their identification we use δ_{532}<5%."

Figure 3. The mixing lines all go through the box that's marked "pollen". This highlights the unavoidable weakness of typing with just two dimensions. Presumably, anything that falls within this box needs context to distinguish between pollen, a pollen mixture, or a smoke-dust mixture that has nothing to do with pollen. Identification by context (particularly where supporting measurements are available) is fine for the purpose of case studies, but there must be significant potential for misidentification in the automated algorithm, I suppose. It would be good to discuss weaknesses as well as strengths of the approach.

Yes, aerosols are always the mixtures. So this problem is attributed not only to the presented, but also to all existing classification algorithms. Next step in our research is the increase of the number of parameters used and quantifications of mixture components.
It is true, that dust – smoke mixture, considered just at one point at depolarization – fluorescence diagram can be recognized as pollen. This is why it is important to consider all the data obtained during the session. We tried to show in this manuscript that the single pixel data for different mixtures provide different patterns, as shown in Fig.3. In our analysis we always observed this kind of patterns, and it helps to get idea about mixture composition.

L268. Clouds are also shown in the aerosol typing masks and line 308 mentions both ice and water droplets, so the thresholds values for ice and water droplets should also be included in Table 1.
Figs 4,5. It's confusing that the ice cloud is only partially included in this example. It's shown in the type mask, but not discussed, and it's not shown in the scatter plot in Fig 5a. It's included in Fig 4, but apparently off-scale. The authors should decide whether they want to include the cloud in their analysis and discussion or not. If not, cut off the plots at an altitude below the cloud. If so, rescale Figure 4, include it in Fig 5 and add discussion about cloud.

The parameters for ice and water particles are added to the Table 1. The ice clouds, however, are normally observed at high altitudes, where fluorescence signal is very weak, so corresponding points at depolarization – fluorescence diagram demonstrate strong scattering. Usually we identified the ice crystals from depolarization measurements only, and this is why we don't show them in Fig.5a. Corresponding comment is added to the revised manuscript.

Figure 5 and similar figures. What's the purpose of the boxes and cross-hairs in the fluorescence vs. depolarization diagrams? The boxes would probably be more useful to readers if they were all the same, and used the values from Table 1. That way, we can see visually how the identified types fall into the broad category already established. I can guess that the crosshairs represent the mean and (probably) standard deviation of identified pure types, but those aren't discussed anywhere in the paper.

In our revised manuscript the boxes correspond to Table 1. The crosses show uncertainty of our measurements, due to statistical errors and uncertainty of calibration. Corresponding comment is added to revised manuscript.

L315-321. The explanation of the smoothing procedure is missing something. Z is a number, but the classification IDs are not numbers that can be added and weighted, but just labels. How are the classifications convolved with Z? Just guessing, I suppose the fluorescence capacity and depolarization ratio are what's averaged using the Z-weightings, and then the classification is done on these smoothed measurements instead? Please clarify in the text.

To make it more clear, we modified corresponding section in the revised manuscript and extended description.
Briefly:
We construct several 'raw' matrices with dimensions equal to primary data matrices (one matrix for each aerosol type (dust, pollen, etc)). If at the first stage some single pixel data point (i,j) is classified as, e.g., pollen, the corresponding value in the 'pollen' matrix is set to 1, otherwise it is set to 0. Then each of these matrices is separately convoluted with the Gauss kernel Z. And, after the convolution, the values for each pixel data (i,j) are being compared. If, e.g., the 'dust' matrix (after the convolution) contains maximal value at the point (i,j) among all the matrices (after the convolution), then the point (i,j) is finally classified as 'dust'.

L339 and 341 and elsewhere. I'd suggest avoiding describing values as "typical" and expand the description to be more specific. For instance, perhaps this is within the ranges seen in your previous publications and/or other publications for cases that have been identified as smoke and urban based on independent data? "Typical" is a bit dangerous, in that it implies a generality that is not established after only a few handfuls of case studies, particularly since the case study identifications seem to mostly be rather dependent on expectations about the typical values. Statements like this unfortunately seem to be quoted and referenced repeatedly so that they become ingrained without becoming better supported. After all, we now know that it is quite common for smoke (in the upper troposphere and stratosphere) to have depolarization values that are much larger than this, and previously published ranges of depolarization for urban aerosol also include significantly larger depolarization values than this.

Agree. We tried to follow this recommendation in revised manuscript
It is true, that aged smoke depolarization ratio at 532 nm in stratosphere can be as high as ~20%. We should mention also, that at 1064 nm the depolarization ratio of smoke in our measurements (even in upper troposphere) never exceeded 5%. This is one more reason to include this depolarization ratio in typing scheme at next stage.

L347. Says that the fluorescence capacity can decrease as a function of relative humidity, explaining a range of variables. Why does it produce variability rather than reducing the fluorescence capacity uniformly?

The water uptake increases the particle backscattering, but does not change the fluorescence. As a result, the fluorescence capacity decreases. The RH, changes with height, which can lead to increase of single pixel data scattering inside the cluster.

L361-367 and Figure 6-7. I agree that the shape of the curve in Figure 7a is very striking and reminiscent of a mixing line. However, I also just read in the previous section that fluorescence capacity is strongly impacted by relative humidity, making me wonder quantitatively how much impact RH has, compared to the impact of mixing. Is there a model (theoretical or empirical) of G_F dependence on relative humidity? The RH profile should be added to Figure 8 (and all the other profile figures). Another aspect that puzzles *and surprises me is the increased G_F specifically in parts of the curtain where the backscatter is lower. This hints that the variation in G_F might be quite strongly related to RH; alternately that the pollen is more diffuse and widespread than the urban aerosol, which I think would be unusual. A curtain of RH (perhaps from MERRA-2 since there is insufficient sonde data to produce a curtain) and/or backtrajectories might help make the scenario more clear.*

Unfortunately, we had no collocated RH measurements. The sonde measurements in UK show that RH increased from 40% to 70% with height. The value of the fluorescence capacity changed for one order of magnitude, and such strong change in G_F can not be explained by the particle hygroscopic growth. For example, from the recent publication of Sicard et al., increase of β_{532} in this RH range for urban aerosol is below factor 1.5. (Sicard, M., Fortunato dos Santos Oliveira, D. C., Muñoz-Porcar, C., Gil-Díaz, C., Comerón, A., Rodríguez-Gómez, A., and Dios Otín, F.: Measurement Report: Spectral and statistical analysis of aerosol hygroscopic growth from multi-wavelength lidar measurements in Barcelona, Spain, Atmos. Chem. Phys. 22, 7681–7697, 2022). Corresponding comment is added to revised manuscript.

The hygroscopic growth can contribute to the backscattering near the PBL top. However, at low altitudes RH is about 40%, so increase of G_F is probably due to decrease of urban particles contribution to the total backscattering (thus pollen contribution becomes more visible).
We tried to use MERRA-2 data, but at low altitudes the modeled parameters differed strongly from observations.

L368-369. It's good that 1064 nm depolarization is included here, because in general, the more data shown, the better the patterns can be understood. However, the text highlights larger values of 1064 nm depolarization to support the inference of pollen, but that's also true for urban aerosol (e.g. Burton et al. 2012). Then "both depolarization ratios decrease with height" as the pollen concentration decreases (L372), but 1064 continues to be larger than 532, so again this is not definitive. Any further comment about this?

Yes, urban aerosol may also have δ_{1064} exceeding δ_{532}. But absolute values of depolarization for pollen are significantly higher. So when at low altitudes we observe high G_F, and high depolarization, the observed $\delta_{1064} > \delta_{532}$ corroborates presence of pollen.

This case and the first case were also included in earlier publications by the same authors. The papers make different analyses of them, so that's fine, but does this mean they also contributed information relevant to producing the ranges used in the algorithm? If so, they are not such good examples to illustrate the performance of the typing algorithm.

The typing is performed on a base of G_F-δ_{532} measurements only. We used these examples, because the aerosol origin was analyzed in our previous publications. Besides, measurements on 30 May 2020 demonstrate very characteristic pattern for urban – pollen mixture.

The vertical profiles of particle parameters for 30 May were presented in our recent paper, so we decided to exclude Fig.8 from revised manuscript. We just provide the reference.

Figure 8 L 715. Why were the profiles created for 21:00-23:00 instead of a later time where the curtain shows pollen at lower altitudes and mixing is discussed? Is this a mistake?

Sorry, this was mistake.

L376-377. I'm not finding the explanation for the lack of variability in the backscatter angstrom exponent to be very convincing. It appears to be saying that the urban particles are growing due to humidification exactly in balance with the effective dry particle size decreasing due to less pollen? (if so, this needs support).
Perhaps some quantitative modeling would help. How small of a backscatter Angstrom exponent would be expected for high concentration of pollen, and just how much contribution to the backscatter is there (based on the mixing model) and how much change in Angstrom would you therefore expect? What confuses me is that the fluorescence capacity also mixes linearly according to the backscatter partition, so if there was really too little backscatter contribution to be noticeable, wouldn't that also mean there would be little variation in G_F as well?

In revised manuscript, this section was completely modified. We agree with reviewer, that behavior of backscatter Angstrom 532/1064 is puzzling. However, the observation presented, could be strongly influenced by hygroscopic growth, which decreases both depolarization and the fluorescence capacity. The backscattering Angstrom exponent strongly (and in complicated way) depends on refractive index, particle size and particle shape. The modeling of the BAE for different mixture compositions is important, but it is out of scope of this research. Just want to mention, that that in publication of Bohlmann et al. (2019) the BAE (at depolarization ratio ~20%) is about 1.0. Which is quite high value and pollen content over Finland is significantly higher than over Lille. So this aspect needs additional research and additional measurements during strong pollen episodes.

L392-393. Unfortunately, the SILAM website only provides current forecast data, so please make the relevant data available as a supplement or shown in a figure. Also, what kind of pollen was it?

In situ measurements at the roof of the building demonstrate presence of significant amount of grass pollen. We added to the revised manuscript (as Appendix) the SILAM maps for four episodes, when presence of pollen was assumed.

L418-419. I'm not quite clear on what the author's intent is here. Is this saying that the algorithm misclassified a mixture as pure urban, or that the mixture only occurs where the classification puts it, but that the two urban layers have quite a lot of difference between them? It would be very helpful (in this case and others) to mark the points in the scatterplots according to the classification result or altitude. I would like to see exactly where the two layers classified as "urban" fall on the apparent mixing line. I think it's interesting that the two layers marked urban have different spectral dependence of depolarization. Backtrajectories would be helpful for this case too, to help understand why the two layers of urban aerosol might have different properties.

To make presentation more clear, we significantly modified this section. First of all, in depolarization – fluorescence diagram in Fig.12 we show the points related to the upper and lower layers by different colors. Back trajectories analysis shows that air masses in both layers are transported from England. So this is probably pollution. Points related to the upper layer are inside the range for ‘urban” aerosol. Points in the lower layer, are partly outside of this range, so the aerosol type is undefined. We assume that this is the mixture of urban and pollen particles, because we have particles with high depolarization and fluorescence capacity (still not high enough to be classified as “pollen”). This mixture is marked by grey color and it is located below 750 m. The maps with SILAM pollen index are added to the revised manuscript as Appendix. On the midnight of 10-11 April 2020 the pollen loading is modeled by SILAM as moderate.
Thus yes, properties of layers are different. Upper layer is urban, while in lower layer below 1 km the urban particles are mixed with pollen.

L420. "typical for urban-pollen mixture". Actually the mixing curve is significantly to the left of the curve in Figure 3, suggesting that the pure pollen in this mixture is not "typical" compared to the ranges given in the table, but is more of an edge case with relatively low fluorescence capacity.

Yes, fluorescence capacity is lower than usual, so this not pure pollen. We added corresponding comment to the text.

L430-436. This is a very nice case to demonstrate contrast in fluorescence between different types. But the type identification is entirely made by inference using the two classification dimensions without any other support such as in situ measurements, backtrajectories, or other lidar-measured quantities like 1064 nm depolarization, lidar ratio or angstrom exponents. It's great that two measurements used for the classification appear to give the ability to make these separations, but for such a key demonstration I think the case studies need to be very well supported. In general I suggest bolstering the verification of the identifications for all the cases (not just this one) by including all relevant data. I mean specifically, first of all, other lidar quantities that have been used in previous classification methodologies, including especially lidar ratios, and also 1064 nm depolarization and angstrom exponents for all cases. Also include RH, backtrajectories and any coincident in situ measurements (especially pollen) for all cases.

In the revised manuscript we added the Table 2, with main intensive particle parameters for all episode considered. The section is modified: we added backtrajectories and analysis of the intensive particle parameters. We have added also Table 3, which compares our observed intensive parameters for dust, smoke, urban with parameters used in existing typing algorithms.

L445 and Figs 15 and 16. The suggested mixing between layers doesn't look convincing. On the fluorescence vs. depolarization diagram, these intermediate points don't follow a nice mixing line like the other mixing cases, and the boundaries in the measurement curtains appear quite crisp. Could these points be artifacts of the smoothing instead?

Yes, at high gradients of backscattering, smoothing sometimes can provide oscillation. We reprocessed this case with decreased smoothing. The threshold value of β_{532} was increased up to 0.3 Mm-1sr-1. Now it is better.

Fig 15. The depolarization especially and perhaps also the fluorescence capacity (outside of the smoke plume) seems to be anti-correlated with backscatter, including in regions that seem unlikely to be pollen-dominated (such as the minimum between the smoke and urban layers). Particulate depolarization is especially susceptible to systematic error, particularly overestimation, at low values of backscatter (Freudenthaler et al. 2009, Burton et al. 2015). Have you done a systematic uncertainty calculation? (Also this is another case where color coding of the scatterplot by altitude would be useful).

Yes, calculation of depolarization at low β_{532} can lead to enhanced uncertainty, especially when high gradients of β_{532} present. In reprocessed data we increased threshold value of β_{532} up to 0.3 Mm-1sr-1. Oscillations decreased. The same is true for fluorescence capacity.
We estimate uncertainty of our depolarization calibration to be below 15%.

Fig 15-18. Include the data for depolarization and angstrom exponent (and RH) for these cases also.

In the revised manuscript we have added Figures 16, 19 with vertical profiles for these episodes.

L455 "G_F increased ... probably due to the mixing with local pollution". Does this make sense? Nothing prior to this in the manuscript suggests that urban pollution has significant fluorescence capacity. Also, on the scatter plot on Figure 18, there's no suggestion that the higher values of G_F in the dust cluster are correlated with depolarization in any way; that is, they are not following any mixing line. What evidence is there that this is not simply normal variability within dust? Table 1 shows dust can have G_F up to 0.5. Why not 0.6? Also, could some of this variability be correlated with RH?

Dust may have very low fluorescence capacity (0.1*10^-4), while urban particles for some episodes had G_F of 0.8*10^-4, or even higher. Thus mixing of dust with pollutions, in principle, can increase the capacity. But reviewer is right, for case presented, the depolarization ratio did not change significantly with height, while capacity strongly decreased in the center of the layer. It can be variation of dust composition (and so the absorption) through the layer. Unfortunately, at this stage we can not make definite conclusion. Corresponding section is strongly modified in revised manuscript.

For the available dust episodes the fluorescence capacity was mainly below 0.5*10^-4. This is why we used it in Table 1. We may reconsider this range, when more data will be available.

Normally properties of dust are not very sensitive to RH. Increase of RH can only decrease the capacity. However at a moment we don't have collocated RH measurements, so unable to make quantitative conclusions about RH influence.

L485. "during Spring-Autumn seasons". It would be helpful to show a timeseries demonstrating that the pollen signature (elevated depolarization and fluorescence capacity) does NOT occur in winter.

We agree, that this would be useful, but it is beyond the scope of this manuscript. Seasonal variation of aerosol composition over Lille will be the topic of separate research.

Typographical or wording:
L19. What is meant by "single" in "first single version of the algorithm". I suggest delete "single" or reword.
Corrected

L18 and L24. Change particle's to particle.
Corrected

L92. Be specific about which wavelength here.
Done

L247. Define LOA.
Done

L270-281. There should be some discussion or at least references to other analyses of mixtures of aerosols that derive similar equations (especially Eq. 7), e.g. Sugimoto and Lee 2006, Gross et al. 2011, Gasteiger et al. 2011, Tesche et al. 2009, Burton et al. 2014.

The references are added. Derivation of Eq.7 looks very straightforward, so probably no explanations are needed.

L280. Eq. 8. It probably would be good to remind the reader that fluorescence capacity and backscatter in this equation refer to particular wavelengths.
Done

L282. "We assume". I think this is meant to refer only to the demonstration in Figure 3, not a general assertion. If true, perhaps swap the first two sentences of the paragraph to make it less likely to be misread. As mentioned in the introduction, the quantities have a lot of variability even within types, so assuming single values wouldn't be well supported.

Done

L300. "the height resolution is 7.5 m". Is that really the resolution or only the grid spacing? That is, taking the detectors into account, are measurements at adjacent vertical grid points independent?

Yes, this is bin resolution of our detection electronics, and in many cases this resolution was used to calculate the particle properties. However, for elevated layers the fluorescence signal was splined. For typing, the Gaussian smoothing procedure was used. Thus ultimate resolution was about 60 m for height and less than 10 minutes for time.

L342. spell out FBC
The section was modified

L344. Add a reference to the reminder. (I think it is Veselovskii 2020?)
Done

L445. Typo in "0.2-0.3"
Corrected

L663-664. It would be helpful to add "using the reference height as Ansmann et al. 1992 (green) or the calibration constant as in Eq 5. (magenta)". (I read figure captions before the text, so having a bit more detail in the captions is very helpful)
Done

L708. Please add clarification to the caption whether the scatter plot shows data for the entire time period shown in the curtain or only the subset that's included in the profile plots of Figure 8.
This is for entire time period. Added to caption.

Figure 2 and 4. There is a lot of red in these plots hinting that the scales might be cutting off the data. Perhaps the scales should be expanded.
Yes, this is because depolarization and backscattering of clouds is very high, comparing to aerosol. We choose such scale, to make details of aerosol more visible. So we would prefer to keep as it is.

Figure 3. Also show the smoke + pollen mixing line, since one of the selected cases references mixing of those two types.
We though to do it, but figure becomes overloaded with curves. Beside, behavior of this mixing line is quite obvious, so we think that it is not so necessary for reader.

Figures 4, 6, 912, 15, 17. It would be helpful if the curtains of intensive properties (depolarization and fluorescence capacity) had consistent scales across each of these plots, making it easier to compare one case to another.
Unfortunately, the cases are very different. In some elevated layers are considered, and in some only the PBL. So we used different scales to show the details. We would prefer to keep different scales for each episode.

References:
Burton, S. P., et al. (2014) Separating mixtures of aerosol types in airborne High Spectral Resolution Lidar data. Atmos. Meas. Tech. 7, 419-436 DOI: 10.5194/amt-7-419-2014
Burton, S. P., et al. (2015) Observations of the spectral dependence of linear particle depolarization ratio of aerosols using NASA Langley airborne High Spectral Resolution Lidar. Atmos. Chem. Phys. 15, 13453-13473 DOI: 10.5194/acp-15-13453-2015

Freudenthaler, V., et al. (2009) Depolarization ratio profiling at several wavelengths in pure Saharan dust during SAMUM 2006. Tellus B 61, 165-179 DOI: 10.1111/j.1600-0889.2008.00396.x
Gasteiger, J. and V. Freudenthaler (2014) Benefit of depolarization ratio at λ = 1064 nm for the retrieval of the aerosol microphysics from lidar measurements. Atmos. Meas. Tech. 7, 3773-3781 DOI: 10.5194/amt-7-3773-2014
Groß, S., et al. (2011) Characterization of Saharan dust, marine aerosols and mixtures of biomass-burning aerosols and dust by means of multi-wavelength depolarization and Raman lidar measurements during SAMUM 2. Tellus B 63, 706-724 DOI: 10.1111/j.1600-0889.2011.00556.x
Sugimoto, N. and C. H. Lee (2006) Characteristics of dust aerosols inferred from lidar depolarization measurements at two wavelengths. Applied Optics 45, 7468-7474 DOI: 10.1364/AO.45.007468
Tesche, M., et al. (2009). "Vertically resolved separation of dust and smoke over Cape Verde using multiwavelength Raman and polarization lidars during Saharan Mineral Dust Experiment 2008." J. Geophys. Res. 114(D13): D13202.

References are added

Response to Reviewer 2

First of all, we would like to thank the Reviewer for reading the manuscript and useful comments.

This paper presents the potentiality of fluorescence measurements in Mie-Raman lidar systems to obtain aerosol type, with focus in biomass, dust, anthropogenic pollution and aerosols. The paper is well structured and discussions are appropriate. In general I am excited about the potential of fluorescence technique for aerosol profile characterizations. However, I agree with previous referee that authors claim the development of an algorithm and that is not straightforward from the paper. Indeed it seems an introduction with different study-cases. So my concerns prior the publication in AMT are:

- There is no mention to the physical principle of fluorescence and if fluorescence can be modeled for different aerosol particles. Maybe these models are not well developed. But if they exist, why not using them for training the model? If not, the authors should clarify this point. In summary, I miss a theoretical background for fluorescence
- The selections of the study cases are excellent, but I miss an overall conclusion that includes all your data. Why not presenting a plot that includes all data and even statistical analyses?

Minor comments

I agree with most of the comments raised by referee 1. I just would like to insist that backward-trajectories and other types of measurements (satellite, in-situ, models) would enrich the discussions. I really miss this information for the cases of Fig 1 and for the pure dust case. Also, the mention to SILAM must be clarified.

In the process of revision, the manuscript was significantly modified. We added a table, containing the particle intensive parameters for the cases considered (lidar ratios at 355 and 532 nm; depolarization ratios at 355, 532 and 1064 nm; and the backscattering and extinction Angstrom exponents). Another table provides the range of variation of particle intensive properties from different typing algorithms for the urban, smoke and dust particles. The table contains also the range of parameters variation for episodes from current study for the same aerosol types. The back-trajectory analysis is included, when the cases are analyzed. In Appendix we added four maps with SILAM pollen index, for the episodes where the presence of the pollen was revealed. Sections 3 and 4 were significantly extended and we hope, that all this improved the manuscript. Details of the manuscript revision are given in our extended response to Reviewer 1.

Reviewer is right, that at this stage we did not analyzed the fluorescence mechanisms. And this should be done at the next step of our research. We plan to increase the number of fluorescence channels, and choose of corresponding spectral intervals will demand this kind of analysis.

Statistical analysis of our observation over Lille is not done yet, but this is definitely one of our goals. And in this manuscript we tried to demonstrate that for different aerosol episode, the depolarization – fluorescence diagram allows to identify the particle type, and it also provides information about the aerosol mixture composition.

Combining of Mie-Raman and fluorescence observations: a step forward in aerosol classification with lidar technology

Igor Veselovskii[1], Qiaoyun Hu[2], Philippe Goloub[2], Thierry Podvin[2], Boris Barchunov[1], Mikhail Korenskii[1]

[1]*Prokhorov General Physics Institute of the Russian Academy of Sciences, Moscow, Russia.*

[2]*Univ. Lille, CNRS, UMR 8518 - LOA - Laboratoire d'Optique Atmosphérique, F-59650 Lille, France*

Correspondence: Qiaoyun Hu (qiaoyun.hu@univ-lille.fr)

Abstract

The paper presents an approach to reveal variability of aerosol type at high spatio-temporal resolution, by combining fluorescence and Mie-Raman lidar observations. The multi-wavelength Mie-Raman lidar system in operation at the ATOLL platform, Laboratoire d'Optique Atmosphérique, University of Lille, includes, since 2019, a wideband fluorescence channel allowing the derivation of the fluorescence backscattering coefficient β_F. The fluorescence capacity G_F, which is the ratio of β_F to the aerosol backscattering coefficient, is an intensive particle property, strongly changing with aerosol type, thus providing a relevant basis for aerosol classification. In this first stage of research, only two intensive properties are used for classification: the particle depolarization ratio at 532 nm, δ_{532}, and the fluorescence capacity, G_F. These properties are considered because they can be derived at high spatio-temporal resolution and are quite specific to each aerosol type. In particular, in this study, we use δ_{532} - G_F diagram to identify smoke, dust, pollen and urban aerosol particles. We applied our new classification approach to lidar data obtained during 2020 – 2021 period, which includes strong smoke, dust and pollen episodes. The particle classification was performed with height resolution about 60 m and temporal resolution better than 8 minutes.

1. Introduction

Atmospheric aerosol is one of the key factors influencing the Earth's radiation budget through absorption and scattering of solar radiation and by affecting cloud formation. The processes of aerosol–radiation and aerosol-cloud interaction depend on aerosol size, shape, morphology, absorption, solubility, etc., thus knowledge of the chemical composition and mixing state of the aerosol particles is important for modeling of aerosol impact (Boucher et al., 2013). The aerosol properties may vary in a wide range, so in practice usually several main types of aerosols are separated on a base of their origin: e.g. urban, dust, marine, biomass burning (Dubovik et al., 2002). Successful remote characterization of column integrated aerosol composition from the observations of Sun – sky photometers and space-borne multiangle polarimeters was demonstrated in numerous publications (Dubovik et al., 2002; Giles et al., 2012; Hamill et al., 2016; Schuster et al., 2016; Li et al., 2019; Zhang et al., 2020). The aerosol impacts, however, depends also on vertical variations/distributions of particle concentration and composition, which cannot be derived from these instruments.

One of the recognized remote sensing techniques for vertical profiling of aerosol properties is a lidar. Multiwavelength Mie-Raman and HSRL (High Spectral Resolution Lidar) lidar systems provide unique opportunity to derive height-resolved particle intensive properties, such as lidar ratios, Angstrom exponents and depolarization ratios at multiple wavelengths. Based on this information, particle type can be determined (Burton et al., 2012, 2013; Groß et al., 2013; Mamouri et al., 2017; Papagiannopoulos et al., 2018; Nicolae et al., 2018; Hara et al., 2018; Voudouri et al., 2019; Wang et al., 2021; Mylonaki et al., 2021 and references therein). However, there is a fundamental difference between particle classification based on the Sun – sky photometer and on lidar observations. From both direct Sun and azimuth scanning measurements of the photometer more than 100 observations are available. From this information the spectrally dependent refractive index and absorption Angstrom exponent can be determined, which is important for aerosol classification (Schuster et al., 2016; Li et al., 2019). The commonly used multiwavelength lidars are based on a tripled Nd:YAG laser and are capable of providing three backscattering (355 nm, 532 nm, 1064 nm), two extinction (355 nm, 532 nm) coefficients and up to three particle depolarization ratios (so called $3\beta+2\alpha+3\delta$ set). Thus the number of available lidar observations is eight or less, which limits the performance of the aerosol typing algorithms. Nevertheless, the results obtained by different research groups demonstrate that lidar-based particle identification is possible. In publications of Burton et al. (2012, 2013) classification was performed from four intensive parameters measured by the HSRL system: the lidar ratio at 532 nm (S_{532}), the backscattering Angstrom exponent for 532/1064 nm wavelengths ($BAE_{532/1064}$), and particle depolarization ratios at 532 nm and 1064 nm (δ_{532}, and δ_{1064}). With these input parameters eight aerosol types: smoke, fresh smoke, urban, polluted maritime, maritime, dusty mix, pure dust and ice were discriminated.

Important information on aerosol vertical distribution comes from the EARLINET/ACTRIS lidar-network, aiming at unifying multiwavelength Mie-Raman lidar systems over Europe (Pappalardo et al., 2014). For the automation of aerosol classification, several approaches were developed in the frame of EARLINET. These approaches include the Mahalanobis distance-based typing algorithm (Papagiannopoulos et al., 2018), a neural network aerosol classification algorithm (NATALI) (Nicolae et al., 2018), and algorithm based on source classification analysis (SCAN) (Mylonaki et al., 2021). All these algorithms have demonstrated their ability for aerosol classification. In particular, the NATALI is able to identify up to 14 aerosol mixtures from $3\beta+2\alpha+1\delta$ observations.

Nevertheless, the above-mentioned algorithms have to deal with a fundamental limitation: the particle intensive properties, even for pure aerosols (generated by a single source) exhibit strong variations. For example, the lidar ratio S_{355} of smoke in publication of Nicolae et al. (2018) varies in 38 sr – 70 sr range, and in our own measurements we observed for aged smoke S_{355} as low as 25 sr (Hu et al., 2021). Strong variation of smoke lidar ratios in EARLINET/ACTRIS observations is discussed also in the recent publication of Adam et al. (2021). Such uncertainty in parameters of the aerosol model complicates the aerosol classification. Thus, it is desirable to combine the Mie-Raman observations with another range resolved technique, providing additional independent information about aerosol composition. Such information can be obtained from laser induced fluorescence emission.

Application of fluorescence lidar technique was intensively considered during the last decade to study aerosol particles. Lidar measurements of the full fluorescence spectrum with multianode photomultipliers (Sugimoto et al., 2012; Reichardt et al., 2014, 2017; Saito et al., 2022) provides an obvious advantage in particle identification. However, even a more simple fluorescence lidar with a single wideband fluorescence channel, opens new opportunities for aerosol characterization (Veselovskii et al., 2021; 2022; Zhang et al., 2021). Such fluorescence configuration could be implemented in existing Mie-Raman lidars, and the fluorescence backscattering coefficient β_F is calculated from the ratio of fluorescence and nitrogen Raman signals. To characterize the aerosol fluorescence properties, the fluorescence capacity G_F is introduced as the ratio of β_F to aerosol backscattering coefficient at one of laser wavelengths

(Veselovskii et al., 2020b). In this study, the backscattering at 532 nm was used. The fluorescence capacity is an intensive particle parameter, which changes strongly with aerosol type, being the highest for smoke and the lowest for dust. Thus, the combination of Mie – Raman and fluorescence backscatter provides a basis to improve particle classification. A Mie – Raman lidar provides several particle intensive parameters, however, the profiles of particle parameters associated with the extinction coefficient, such as lidar ratio or extinction Angstrom exponent, may contain strong noises, because the extinction coefficients are derived from the slope of Raman lidar signals, thus averaging over significant spatio-temporal intervals is demanded. Meanwhile, the particle depolarization and the fluorescence *capacity* can be calculated with high spatio-temporal resolution.

Recently, we have demonstrated that the $\delta - G_F$ diagram allows to separate several aerosol types, such as dust, pollen, urban (continental) and smoke (Veselovskii et al., 2021a). In the present study, we use this technique to classify aerosol particle types in the troposphere at high spatio-temporal resolution. We present results of aerosol classification on the basis of fluorescence and Mie-Raman lidar measurements performed at the ATOLL (ATmospheric Observation at liLLe) at Laboratoire d'Optique Atmosphérique, University of Lille, during 2020 – 2021 period, which includes strong smoke, dust and pollen episodes. Paper starts with a description of the experimental setup and data processing scheme in Sect.2. In Sect.3 we present the algorithm for aerosol classification on a base of depolarization and fluorescence measurements. Results of the application of the developed approach to different atmospheric situations, including smoke, dust and pollen episodes are given in Sect.4.

2. Experimental setup and data analysis

2.1. Lidar system

The multiwavelength Mie-Raman lidar LILAS (LIlle Lidar AtmosphereS) is based on a tripled Nd:YAG laser with a 20 Hz repetition rate and pulse energy of 70 mJ at 355 nm. Backscattered light is collected by a 40 cm aperture Newtonian telescope and the lidar signals are digitized with Licel transient recorders with 7.5 m range resolution, allowing simultaneous detection in the analog and photon counting mode. The system is designed for the detection of elastic and Raman backscattering, allowing the so called $3\beta+2\alpha+3\delta$ data configuration, including three particle backscattering (β_{355}, β_{532}, β_{1064}), two extinction (α_{355}, α_{532}) coefficients along with three particle depolarization ratios (δ_{355}, δ_{532}, δ_{1064}). The particle depolarization ratio, determined as a ratio of cross- and co-polarized components of the particle backscattering coefficient, was calculated and calibrated in the same way as described in Freudenthaler et al. (2009). Many calibration and operation procedures have been automated for the LILAS system to improve the overall performance of the lidar in terms of observation frequency and data quality. The aerosol extinction and backscattering coefficients at 355 and 532 nm were calculated from Mie-Raman observations (Ansmann et al., 1992), while β_{1064} was derived by the Klett method (Klett, 1985). The full geometrical overlap was achieved at approximately 750 m range. For calculation of α and β at 532 nm we use the rotational Raman scattering instead of the vibrational one (Veselovskii et al., 2015), which allows to increase the power of Raman backscatter and to decrease separation between the wavelengths of elastic and Raman components. Additional information about atmospheric parameters was available from radiosonde measurements performed at Herstmonceux (UK) and Beauvechain (Belgium) stations, located 160 km and 80 km away from the observation site respectively.

The LILAS system can also profile the laser induced fluorescence of aerosol particles. A part of the fluorescence spectrum is selected by a wideband interference filter of 44 nm width centered at 466 nm. The strong sunlight background at daytime restricts the fluorescence observations to nighttime hours. The fluorescence backscattering coefficient β_F, is calculated from the ratio of fluorescence and nitrogen Raman backscattering signal, as described in Veselovskii et al. (2020b). This approach allows us to evaluate the absolute values of β_F, if the relative sensitivity of the channels is calibrated and the nitrogen Raman scattering differential cross section is known. All β_F profiles presented in this work were smoothed with the Savitzky – Golay method, using second order polynomials with 21 points in the window. For the calculation of the fluorescence capacity G_F, in principle, backscattering coefficients at any laser wavelength can be used. In our study we always used β_{532}, because it is calculated with the use of rotational Raman component and is considered to be the most reliable, thus the fluorescence capacity is calculated as $G_F = \frac{\beta_F}{\beta_{532}}$.

2.2.Calculation of the particle backscattering coefficient from Mie-Raman measurements

Mie – Raman lidar measurements allow independent evaluation of aerosol extinction and backscattering coefficients. Commonly used approach for β calculation was formulated in the paper of Ansmann et al. (1992). This approach includes the choice of a reference height, where the scattering is purely molecular. However, such height range is not always available, for example, in the presence of the low level clouds. Moreover, when long-term spatio-temporal variations of backscattering coefficients are analyzed, the uncertainty in the choice of the reference height leads to oscillations in β profiles. To resolve this issue, we modified the Raman method as described below.

In an elastic channel, the backscattered radiative power P_L, at wavelength λ_0 and distance z is described by the lidar equation:

$$P_L = O(z)\frac{1}{z^2}C_L(\beta_L^a + \beta_L^m)\exp\left\{-2\int_0^z(\alpha_L^a + \alpha_L^m)dz'\right\} = O(z)\frac{1}{z^2}C_L(\beta_L^a + \beta_L^m)T_L^2\,, \qquad (1)$$

while in a Raman channel, it can be written as:

$$P_R = O(z)\frac{1}{z^2}C_R\beta_R\exp\left\{-\int_0^z(\alpha_L^a + \alpha_R^a + \alpha_L^m + \alpha_R^m)dz'\right\} = O(z)\frac{1}{z^2}C_R\beta_R T_L T_R\,. \qquad (2)$$

Here O(z) is the geometrical overlap factor, which is assumed to be the same for elastic and Raman channels. C_L and C_R are the range independent constants, including efficiency of the detection channel. T_L and T_R are one-way transmissions, describing light losses on the way from the lidar to distance z at laser λ_L and Raman λ_R wavelengths. Backscattering and extinction coefficients contain aerosol and molecular contributions: $\beta_L^a + \beta_L^m$ and $\alpha_L^a + \alpha_L^m$, where the superscripts "*a*" and "*m*" indicate aerosol and molecular scattering, respectively. Raman backscattering coefficient is:

$$\beta_R = N\sigma_R\,, \qquad (3)$$

where N is the number of Raman scatters (per unit of volume) and σ_R is the Raman differential scattering cross section in the backward direction.

Dividing equation (1) on (2) we get:

$$\frac{P_L}{P_R} = \frac{C_L}{C_R}\frac{(\beta_L^a + \beta_L^m)}{\beta_R}\frac{T_L}{T_R} \qquad (4)$$

Backscattering coefficient is calculated from (3) and (4) as:

$$\beta_L^a = \frac{P_L}{P_R}\frac{C_R}{C_L}\sigma_R N\frac{T_R}{T_L} - \beta_L^m = \frac{P_L}{P_R}KN\frac{T_R}{T_L} - \beta_L^m \qquad (5)$$

The differential transmission $\frac{T_L}{T_R}$ can be calculated the same way, as it is done for the water vapor measurements (Whiteman, 2003). For rotational Raman signal, which we use in our 532 nm channel (Veselovskii et al., 2015), $\lambda_L \approx \lambda_R$, so $\frac{T_L}{T_R}=1$.

The calibration constant $K=\frac{C_R}{C_L}\sigma_R$ can be found by comparing β_L^a in Eq.5 with the backscattering coefficient $\tilde{\beta}_L^a$ computed with the traditional Raman method, using the reference height (Ansmann et al., 1992).

$$K=(\tilde{\beta}_L^a+\beta_L^m)\frac{P_R}{P_L}\frac{1}{N}\frac{T_L}{T_R} \tag{6}$$

For simplicity, hereinafter we will use notation β_L instead β_L^a. Thus, if during the measurement session we have a temporal interval, where the reference height is available, we can determine the calibration constant K and use it for β_L calculations from eq.5, assuming that relative sensitivity of channels during the session is not changed. Even if cloud layers occur during the whole session, we can use K from the previous cloud-free profiles (assuming, again, that the relative sensitivity of channels is the same). We will call this approach for β calculation as “modified Raman method”, to distinguish it from traditional one (Ansmann et al., 1992).

To estimate variations of the relative sensitivity of the channels, we analyzed long-term cloudless measurements when the reference height was available for every individual profile. The results demonstrate that variations of calibration constant during the session (about 8 hours) were below 3%. Fig.1 and 2 present the application of this modified Raman method to the measurements on 2 March 2021. The dust layer extended from 2 km to 8 km height and inside this layer the ice and liquid clouds were formed during the 00:00 – 05:00 UTC interval, thus β_{532} could not be calculated with traditional Raman technique. The temporal interval 19:00 – 20:00 was used to find calibration constant K. Fig.1 shows vertical profiles of backscattering coefficient $\tilde{\beta}_{532}$ calculated with traditional Raman method (with reference height), and β_{532} calculated with modified method (with the calibration constant). Profiles of $\tilde{\beta}_{532}$ and β_{532} coincide for the whole height range. The calibration constant K, shown on the same plot, does not demonstrate height dependence, though oscillations around the mean value increase with height. For computations, we choose the value of K at low altitudes averaged inside some height interval.

Fig.2 provides spatio-temporal variations of β_{532}, particle depolarization δ_{532} and the fluorescence capacity G_F. Depolarization measurements reveal the presence of dust ($\delta_{532}\approx 30\%$) and the ice cloud above 4 km ($\delta_{532}>40\%$). The liquid cloud below 4 km after midnight can be identified by a low depolarization ratio $\delta_{532}<3\%$. The fluorescence capacity of dust is low, about 0.2×10^{-4}. However, below 2 km, G_F is significantly higher, up to 1.2×10^{-4}. In combination with a high depolarization ratio (up to 20%), it can indicate the presence of pollen at low altitudes. On the fluorescence capacity panel, we can see that after 01:00 UTC the dust and pollen layers are mixed below 2 km, resulting in a value of G_F about 0.5×10^{-4}. The fluorescence capacity inside ice and liquid clouds is below 0.01×10^{-4}. Fig.2 clearly demonstrates the advantage of simultaneous depolarization and fluorescence measurements for the study of cloud formation in the presence of aerosol. All spatio-temporal distributions of β_{532} presented in this paper were calculated from Eq.5 with a modified Raman method.

3. Aerosol classification based on fluorescence measurements

3.1. *Approach for aerosol classification*.

As was discussed in our recent publication (Veselovskii et al., 2021), the δ-G_F diagram allows to separate several aerosol types, including smoke, dust, pollen, urban, ice and liquid water particles. Smoke and urban aerosols both have a small depolarization ratio, but the fluorescence capacity of smoke is almost one order higher, so these particles can be separated. Dust and pollen both have high depolarization ratio (up to 30%), but G_F of dust is significantly lower, which again provides basis for discrimination. The depolarization ratio of some aerosol types is characterized by strong spectral dependence. For example, the depolarization ratio of aged smoke decreases with wavelength. It is below 5% at 1064 nm but at 355 nm in upper troposphere it may exceed 20% (Burton et al., 2015; Haarig et al., 2018; Hu et al., 2019; Veselovskii et al., 2022), which complicates smoke and dust separation. For pollen, on the contrary, the depolarization ratio at 1064 nm can be the highest (Veselovskii et al., 2021). Thus, choice of δ_{1064} for δ-G_F diagram could be advantageous. However, as mentioned, the backscattering coefficient at 1064 nm is calculated with Klett method (Klett, 1985), which, besides assumption about lidar ratio, needs reference height and cannot be used in cloudy situations. This is why in our study we used the δ_{532}-G_F diagram.

In our present work, we consider a simple classification scheme since we use only two intensive parameters G_F and δ_{532}. Our goal is to demonstrate that in the δ_{532}-G_F diagram, our lidar observations form clusters and characteristic patterns which can be attributed to different aerosol types or their mixtures. We consider four aerosol types: dust, smoke, pollen and urban, and two cloud types: liquid and ice clouds. Dust and pollen are large particles of complicated shape, characterized by high depolarization ratio, while smoke and urban pollution are small particles with low depolarization. In our classification "urban aerosol" includes continental aerosol, sulfates and soot. At this stage, we do not yet consider absorption to discriminate particles.

The choice of the range of particle properties variation for each aerosol type is an important aspect of the approach. Typical ranges of G_F and δ_{532} variations used in our classification scheme are given in Table 1 and are shown in Fig.3. These ranges are based on results obtained in LOA (Laboratoire d'Optique Atmosphérique) and on results presented in aerosol classification studies (Burton et al., 2012, 2013; Nicolae et al., 2018; Papagiannopoulos et al., 2018, Mylonaki et al., 2021).

Dust. The depolarization ratio, δ_{532}, of Saharan dust near the source regions is up to 35% (Veselovskii et al., 2020a). However, after transportation and mixing with local aerosol δ_{532} can be as low as 20% (Rittmeister et al., 2017). In many studies, the dust events having with smaller depolarization ratio are classified as "polluted dust" (e.g. Burton et al., 2012, 2013). At the moment, we do not introduce the discrimination between the two subtypes and mark as "dust" the particles with 20%<δ_{532}<35%, and 0.1×10^{-4}<G_F <0.5×10^{-4}.

Smoke. In 2021-2022, we regularly observed, over ATOLL platform, smoke layers originated from Californian and Canadian forest fires (Hu et al., 2022). The particle depolarization and fluorescence capacity of this transported smoke varied from episode to episode and, for classification, we selected the ranges 2%<δ_{532}<10%, 2×10^{-4}<G_F <6×10^{-4}. At this stage, we do not discriminate "fresh" and "aged" smoke, and the range of δ_{532} variation is similar to the one used in classification of Burton et al. (2012).

Pollen. The pollen over north of France is usually mixed with other aerosol and the particles which we mark as "pollen" are actually the mixtures. Depolarization ratio of clean pollen varies strongly for different taxa. For birch pollen, Cao et al. (2010) reported δ_{532}=33%, and in the measurements over Finland during birch pollination (Bohlmann et al., 2019), observed values of δ_{532} up to 26%. The observations over Lille during pollen season (Veselovskii et al., 2021a) rarely revealed values δ_{532} exceeding 20%. Based on that observations, we type as "pollen" the particles mixtures with 15%<δ_{532}<30%, and $0.8\times10^{-4}<G_F<3.0\times10^{-4}$.

Urban. This type of aerosol includes a variety of particle types (e.g. sulfates, soot) and its properties may depend on the relative humidity. Based on our measurements inside the boundary layer, for classification we choose the ranges 1%<δ_{532}<10%, and $0.1\times10^{-4}<G_F<1.0\times10^{-4}$. Similar range for δ_{532} is used in classification of Burton et al. (2013). Urban and smoke particles both have a low depolarization, but the smoke fluorescence capacity can be up to one order higher, so these particles can be reliably discriminated.

Ice and water clouds. Both cloud types have low fluorescence capacity $G_F<0.01\times10^{-4}$. However, the ice clouds are usually observed at the heights, where fluorescence signal is low and can not be used for classification. Thus above ~8 km, the ice cloud are identified by high depolarization ratio δ_{532}>40%. Depolarization ratio of the liquid water clouds is usually affected by the effects of the multiple scattering, so for their identification we use δ_{532}<5%.

The analysis of aerosol mixtures is an important subject and, the possibility to separate the mixture components based on lidar measurements was discussed in publications of Sugimoto and Lee (2006), Gross et al. (2011), Gasteiger et al. (2011), Tesche et al. (2009), Burton et al. (2014). The information about mixture composition can be also revealed in δ_{532}-G_F diagram. For example, pollen can be mixed with urban particles. At different heights the pollen contributes differently to β_{532}, so at δ_{532}-G_F diagram, the data points will form the pattern, which extends from location, attributed to "pure" urban aerosol to location, attributed to "pure" pollen. To estimate, how such pattern looks like, a simplified modeling for fixed particle parameters was performed. Corresponding results are shown in Fig.3 by symbols (circles). The particle depolarization ratio δ of the mixture, containing urban aerosol (u) and pollen (p), with depolarization ratios δ^u and δ^p, can be calculated as:

$$\delta = \frac{\left(\frac{\delta^p}{1+\delta^p}\right)\beta^p + \left(\frac{\delta^u}{1+\delta^u}\right)\beta^u}{\frac{\beta^p}{1+\delta^p} + \frac{\beta^u}{1+\delta^u}} \tag{7}$$

The fluorescence capacity of the mixture is given by:

$$G_F = \frac{\beta^u G_F^u + \beta^p G_F^p}{\beta} \quad (8)$$

Here total backscattering $\beta = \beta^u + \beta^p$.

The computations in Fig.3 were performed for values of pollen contribution $\frac{\beta_{532}^p}{\beta_{532}}$ in 0 - 1.0 range with step 0.1. We assume that the depolarization ratios of pollen and urban aerosol are δ_{532}^p =30% and δ_{532}^u =3%, while the fluorescence capacities are G_F^u =0.2×10^{-4} and G_F^p =2.5×10^{-4}. We remind that the fluorescence capacities are calculated at 532 nm wavelength. In the δ_{532}-G_F diagram the computed points provide a characteristic curve, which in the next section will be compared with experimental results. The same computations were performed for a smoke (s) and dust (d) mixture, assuming δ_{532}^d =30%, δ_{532}^s =3%, G_F^d =0.2×10^{-4} and G_F^s =4.0×10$^{-4.}$ Corresponding results are shown in Fig.3 with stars. In a similar way, the characteristic curves for other mixtures can be also represented.

We are also able to identify liquid water and ice layers. Liquid water cloud layers have low fluorescence capacity (G_F<0.01×10^{-4}) and δ_{532}<3%. Ice particles also have low G_F, but at heights where ice clouds are usually observed, the signal of fluorescence backscattering is noisy. Thus at high altitudes ice particles are discriminated by a high depolarization ratio δ_{532}>40 %.

3.2. ***Classification of spatio-temporal observations***

The input parameters in our classification scheme are the spatio-temporal distributions of β_{532}, δ_{532} and G_F, which are presented as matrices $\beta_{532}^{i,j}$, $\delta_{532}^{i,j}$, $G_F^{i,j}$, where i=1… N_T; j=1… N_H. Values N_T and N_H are the numbers of temporal and height intervals in the analyzed dataset. In a single measurement we accumulate 2×10^3 laser pulses, so temporal resolution of the measurements is about 100 s, while the height resolution is 7.5 m.

The particle intensive properties cannot be evaluated reliably when the backscattering coefficient is low. Thus, we set a threshold value for β_{532} (normally 0.2 Mm^{-1}sr^{-1}); namely, when $\beta_{532}^{i,j}$< 0.2 Mm^{-1}sr^{-1} the elements of the matrices $\delta_{532}^{i,j}$ and $G_F^{i,j}$, are classified as "low signal" and ignored. For the remaining elements, we determine the aerosol type, using our approach. A primary typing is being made for each point *(i,j)* separately, in accordance with parameter ranges given in the Table 1. The elements, which are out of all these ranges, are marked as “undefined”. We consider 6 types of the particles, respectively dust, smoke, pollen, urban, ice crystals and water droplets. Moreover, there can be two additional results of primary typing: “undefined” and “low signal”. Thus, there are altogether 8 possible results of primary typing. For every aerosol type, a $N_T \times N_H$ dimension matrix is constructed. If at this first stage of classification some single pixel point (i, j) is classified as, e.g., dust, the corresponding value in the 'dust' matrix is set to 1, otherwise it is set to 0.

The single pixel particle parameters contain statistical noise, which influences the results of the primary typing, thus producing high frequency oscillations of non-physical character. From a physical point of view, the aerosol single-type areas should form smooth regions, so a special smoothing procedure (stage 2 of our algorithm) was developed to remove the oscillations. The smoothing procedure is based on a convolution with Gaussian kernel

$$Z = \exp\left(-\left(\frac{t^2}{s_T^2} + \frac{h^2}{s_H^2}\right)\right) \qquad (9)$$

where t and h are temporal and height coordinates. The resolution of typing is being controlled by the parameters s_T and s_H, which are set as the number of temporal and height bins.

On the second stage of classification each of these matrices is separately convoluted with the Gauss kernel Z. After the convolution, the values for each pixel (i,j) are being compared. If, e.g., the 'dust' matrix contains maximal value at the pixel (i,j), in respect to all other matrices, then the pixel (i,j) is finally classified as dust. The choice of smoothing parameters depends on aerosol loading and aerosol type. For the measurements inside the boundary layer in many cases the single pixel typing (s_T=1, s_H=1) is possible, while for analysis of the weak elevated layers the smoothing should be applied. All results presented in this study were obtained for s_T=3 and s_H=5, thus the temporal and range resolutions of our typing procedure are estimated to be about 8 minutes and 60 m respectively.

4. *Application of classification approach to LILAS data*

The classification approach, described in the previous section, was applied to the data of the Mie-Raman- Fluorescence lidar at the ATOLL platform, located on the campus of Lille University, during 2020 – 2021 period. Here we present results of aerosol classification for several relevant atmospheric situations, to demonstrate that different aerosol types are well separated based on δ_{532}-G_F diagram.

12 September 2020: Wildfire smoke

Fig.4 presents the spatio-temporal variations of aerosol and fluorescence backscattering coefficients (β_{532} and β_F) together with the particle depolarization ratio δ_{532} and the fluorescence capacity G_F during smoke episode on the night 12-13 September 2020. The smoke layer extends from approximately 2 km to 5 km height, and it is characterized by high fluorescence capacity G_F>3.0×10^{-4} and low depolarization ratio δ_{532}<7%. The cirrus clouds occurred above 11 km height during the whole night. The smoke layer was transported from North America; detailed analysis of the layer origin and transportation is given in the recent publication of Hu et al. (2022). The results of aerosol typing for this episode are shown in Fig.5. On the δ_{532}-G_F diagram these data form two clusters. First cluster includes points in the range $2.0\times10^{-4}<G_F<6.0\times10^{-4}$ and $2\%<\delta_{532}<7\%$, such high fluorescence and low depolarization should be attributed to smoke particles. The second cluster consists of points localized inside $0.1\times10^{-4}<G_F<0.8\times10^{-4}$ and $1\%<\delta_{532}<3\%$ intervals which corresponds to urban particles in Table 1. After cluster localization, the observations can be plotted as aerosol types, using the parameters in Table 1 and the approach, described in section 3.2. The aerosol types in Fig.5b are spatially separated and contain no high frequency oscillations. Urban particles are localized at low heights, below 1 km. We would like to remind that, at the condition of high relative humidity (RH), the fluorescence capacity can decrease due to the particle's hygroscopic growth (Veselovskii et al., 2020). In accordance with radiosonde data the relative humidity below 1 km was quite high (about 70% at 500 m) and decreased with height, which can explain the wide range of G_F variation observed for urban particles in Fig.5a.

The particle intensive properties, such as the lidar ratios at 355 nm and 532 nm wavelengths (S_{355}, S_{532}), the particle depolarization ratios (δ_{355}, δ_{532}, δ_{1064}), the extinction ($A^{\alpha}_{355/532}$) and the backscattering ($A^{\beta}_{355/532}$, $A^{\beta}_{532/1064}$) Angstrom exponents for the episodes analyzed in this study, are summarized in Table 2. For this measurement session, in the smoke layer the lidar ratio at 532 nm significantly exceeds corresponding value at 355 nm (S_{532}=80±12 sr and S_{355}=50±7 sr). The particle depolarization ratio decreases with wavelength from 4.5% at 355 nm to 2% at 1064 nm. Such spectral dependence of the lidar ratio and depolarization ratio for the aged smoke is in agreement with previous studies (e.g. Haarig et al., 2018; Hu et al., 2022 and references therein).

30 May 2020: Urban vs Pollen

Pollen grains represent a significant fraction of primary biological materials in the troposphere and fluorescence induced emission provides an opportunity for their identification. Fig.6 presents spatio-temporal variations of β_{532}, β_F, δ_{532}, G_F during pollen season on the night 30-31 May 2020. Presence of different types of pollen over Lille in Spring – Summer 2020 was discussed in our recent publication (Veselovskii et al., 2021). In particular, on 30 May 2020 the in situ measurements at the roof of the building demonstrate the presence of significant amount of grass pollen. The transport of pollen can be analyzed with a global-to-meso-scale dispersion model SILAM (Sofiev et al., 2015). In Appendix we show the maps of the pollen index, for four sessions from this study at 22 UTC. On 30 May the pollen index in Lille region is about 5.0, indicating high content of pollen.

The aerosol is located inside the planetary boundary layer (PBL) below 2.5 km. At altitudes below 1 km, the depolarization ratio δ_{532} after 23:00 increases up to ~15% simultaneously with an increase of the fluorescence capacity up to 2.0×10^{-4}, which can be an indication of pollen presence. On the δ_{532}-G_F diagram in Fig.7a, the single pixel data points spread from the values typical for the urban particles to the values typical for the pollen. Contribution of pollen to the total backscattering changes with height and the points form the pattern, similar to characteristic curve, calculated for urban – pollen mixture in Fig.3. In accordance with radiosonde data from Herstmonceux station, the RH at midnight was about 40% at 500 m and it increased up to 70% at 2000 m, thus the spatio – temporal variations of RH could influence the observed values of the backscattering coefficient and depolarization ratio. In particular, the hygroscopic growth can decrease the values of both δ_{532} and G_F. However, the value of the fluorescence capacity in Fig.7a changes for almost one order of magnitude, and such strong change in G_F can not be explained by the particle hygroscopic growth only. For example, from the recent publication of Sicard et al. (2022), increase of β_{532} of urban aerosol for this range of RH, is below the factor 1.5. Thus, we suppose that the pattern in Fig.7a is due to the mixing urban and pollen particles The spatio–temporal distribution of aerosol types is shown in Fig.7b. The urban particles (brown) are predominant, while pollen (yellow) is localized below 1 km height. The grey color corresponds to unidentified aerosol type which, in our case, is the mixture of urban particles and pollen.

An indicator of pollen presence in an aerosol mixture, along with high depolarization ratio, can be a higher value of δ_{1064} in respect to δ_{532} or δ_{355} (Cao et al., 2010; Veselovskii et al., 2021).

Vertical profiles of the particle depolarization ratio at all three wavelengths for this episode are given in Fig.8c of Veselovskii et al. (2021). At 0.75 km height, where δ_{1064} is about 15%, the ratio $\frac{\delta_{1064}}{\delta_{532}}$ is 1.5, which corroborates suggestions about pollen presence. For urban aerosol the depolarization spectral ratio $\frac{\delta_{1064}}{\delta_{532}}$ can be also above 1.0 (Burton et al., 2013), but absolute values of depolarization are significantly lower than for pollen particles (below 10%).

14 September 2020: wildfire smoke vs pollen mixture

Another strong smoke episode occurred in the night 14-15 September 2020, and corresponding distributions of β_{532}, β_F, δ_{532}, and G_F are shown Fig.8. The elevated smoke layer with low depolarization ratio (δ_{532}<5%) and high fluorescence capacity (up to 4.0×10^{-4}) was observed at approximately 6 km height during the whole night. Inside the boundary layer the depolarization ratio is higher, up to 15%, while fluorescence capacity is lower (about 1.0×10^{-4}), compared to the elevated layer. On the δ_{532}-G_F diagram in Fig.9a we can see the cluster of data points, corresponding to the smoke. The same time, a part of the points are inside the range of parameters attributed to the pollen (Table 1). The remaining points should be attributed to the mixture of pollen, smoke and urban aerosol. On the distribution of the particle types (Fig.9b) this mixture is marked with gray color. The pollen particles are localized below 1 km. Presence of pollen over Lille in September is not common, but it can be transported from other regions. The SILAM pollen index in Fig.A1 for this date demonstrates the transport of pollen to northern France from the southeast of France and the east Mediterranean.

Fig.10a presents profiles of δ_{532} and δ_{1064} together with β_{532} for the temporal interval 00:00 – 04:00 UTC. The relative humidity, in accordance with radiosonde data from Herstmonceux station, did not exceed 50% below 1.7 km. Above that height RH increased up to 75% at 2.5 km, thus the observed increase of β_{532} above 1.5 km can be partly related to RH growth. The relative humidity inside the smoke layer did not exceed 10%. Similarly to Fig.8, δ_{1064} exceeds δ_{532} at low heights. The ratio $\frac{\delta_{1064}}{\delta_{532}}$ is about 1.5 at 1 km and inside the smoke layer $\frac{\delta_{1064}}{\delta_{532}} \approx 0.4$. Higher values of depolarization ratio at 532 nm compared to 1064 nm are reported for aged smoke by Haarig at al. (2018), Hu et al. (2019, 2022). The BAE does not present significant height variations: $A^{\beta}_{532/1064}$

is about 1.0 inside the PBL and it increases to 1.25 inside the smoke layer (Fig.10b). Simultaneously, the fluorescence capacity in the smoke layer increases about a factor 4, comparing to the PBL, which demonstrates efficiency of the fluorescence technique for discriminating smoke from other aerosol types.

10 April 2020: Urban vs Pollen

In the beginning of April, we experienced several atmospheric situations, for which elevated layers were classified as urban aerosols. One of such cases, on the night 10 -11 April 2020, is shown in Fig.11. Lidar observations were performed at an angle of 45 degrees to the horizontal, so the minimum height reachable in the analysis is 350 m. The relative humidity, in accordance with radiosonde data from Herstmonceux station, increased with height from 54% at 1.0 km to 65% at 2.2 km. The layer with depolarization ratio δ_{532} below 5% was observed at about 2 km height during the night. The fluorescence capacity in the layer is low (below 0.5×10^{-4}), so it is identified as urban aerosol. HYSPLIT backward trajectories (not shown) indicate that the air masses at 750 m and 2000 m heights were transported from England (HYSPLIT, 2022). For the period 21:00 – 23:00 UTC the depolarization ratio below 500 m has increased simultaneously with the fluorescence capacity, which can be an indication of pollen presence.

On the δ_{532}-G_F diagram (Fig.12a) the single pixel measurements in 350 m – 1500 m and 1500 m – 2500 m height ranges are shown by different colors. The data points related to the upper layer are within the range of parameters expected for urban aerosol. The points in the lower layer (below 1500 m), are partly out of this range, so the aerosol type for these points is undefined. We assume that this is the mixture of urban and pollen particles, because we observe particles with high depolarization (δ_{532}>15%) and fluorescence capacity up to 0.7×10^{-4}. This mixture is marked by grey color on aerosol mask in Fig.12b. The pollen index provided by SILAM over Lille on the midnight, is above 4.0, so the presence of pollen particles is expectable.

The presence of pollen is supported also by the profiles of δ_{532} and δ_{1064}, shown in Fig.13. At low heights δ_{1064} exceeds δ_{532} and the ratio $\frac{\delta_{1064}}{\delta_{532}}$ is about 1.4 at 0.5 km. However, inside the elevated layer this ratio decreases and becomes about 0.8 at 2.25 km, which indicates that mixture composition changed. For the same height range, the fluorescence capacity decreases from $0.6\times10^{-}$

^{4} to 0.3×10^{-4} while $A^{\beta}_{532/1064}$ gradually increases from 0.75 to 1.25 which can be due to decrease of pollen contribution.

As follows from Table 2, in the lower layer the values of S_{355} and S_{532} are close (about 48±7 sr). However, in elevated layer S_{532} increases to 70±7 sr, while S_{355} remains the same. Higher values of S_{532}, in respect to S_{355}, are typical for aged smoke (e.g. Müller et al., 2005; Hu et al., 2022). Moreover, $A^{\beta}_{355/532}$ significantly exceeds $A^{\alpha}_{355/532}$, which was also reported for aged smoke. Thus, based on intensive properties only, we could classify this layer as “smoke”. However, due to low fluorescence capacity, in our approach we identify it as “urban”.

11 August 2021: contacting layers of smoke and urban aerosol

Separation of smoke and urban particles is a challenging task for Mie – Raman lidar, because both types have small effective radius, and similar depolarization ratios δ_{532}. However, the fluorescence capacity of smoke is about factor 4-5 higher than that of urban aerosol, which allows their reliable separation. The analyses of the measurements in the night 11-12 August 2021 are shown in Fig.14. The RH decreases with height from 70% to 40% inside 500 m – 2250 m range. The main part of aerosol is concentrated below 2500 m and two height intervals can be distinguished. Above approximately 1500 m the layer with high fluorescence capacity (up to 3.0×10^{-4}) is observed, while in the layer below 1500 m, the G_F is low, (below 0.8×10^{-4}). HYSPLIT backward trajectories (not shown) indicate that the air masses at 1800 m heights were transported from North America, so these may contain wield fire smoke.

On the δ_{532}-G_F diagram (Fig.15a) the single pixel measurements in 500 m – 1400 m and 1400 m – 2500 m height ranges are shown by different colors. The cluster of points, corresponding to the upper layer, is localized mainly inside the interval 1.8×10^{-4}<G_F<4.0×10^{-4} and 4%<δ_{532}<10%, and can be attributed to smoke. The points corresponding to the lower layer are partly identified as urban particles, but a part of the points is out of the range and forms a pattern typical for urban – pollen mixture. The SILAM pollen index in Fig.A1 is above 5.0, so contribution of pollen can be noticeable. The smoke and urban layers are in contact and the particle mixing occurs, which increases dispersion within the clusters.

Vertical profiles of δ_{532} and $A^{\beta}_{532/1064}$ in Fig.16 do not demonstrate significant difference for upper and lower layers. Meanwhile, the fluorescence capacity increases by factor 4. The lidar ratios

S_{355} and S_{532} in the upper layer, as follows from Table 2, are 45±7 sr and 72±11 sr respectively. The $A^{\beta}_{355/532}$ significantly exceeds $A^{\alpha}_{355/532}$ (2.2±0.2 and 1.0±0.2 respectively), so based on intensive parameters, the upper layer can be also identified as smoke.

1 April 2021: Dust

Dust layers transported from Africa are regularly observed over North of France. One such dust episode took place in the night 1-2 April 2021 and the corresponding spatio-temporal variations of β_{532}, β_F, δ_{532}, and G_F are shown in Fig.17. The dust layer, with depolarization ratio exceeding 30%, and low fluorescence, extends from approximately 1.0 km to 5.0 km height. The fluorescence capacity varied inside the layer. In the center it was the lowest (about 0.1×10^{-4}), but at the bottom of the layer and near the top, G_F increased up to (0.2÷0.3) $\times10^{-4}$. In Fig.18a, (δ_{532}-G_F diagram), we observe a cluster of particles, which can be identified as dust. There is also a second small cluster, attributed to urban aerosols. On the distribution of particle types in Fig.18b the urban aerosol occurs below 800 m after 23:00 UTC.

Fig.19 provides vertical profiles of β_{532}, δ_{532}, δ_{355}, β_F, G_F and $A^{\beta}_{355/532}$. Measurements at 1064 nm were not available for this episode. Depolarization ratios at 355 nm and 532 nm are close to 30% through the layer, though at heights below 1.5 km there is small enhancement of δ_{532} up to 34%. The fluorescence capacity is about 0.4×10^{-4} at 1.5 km and it decreases with height to 0.1×10^{-4} at 2.5 km. However, this decrease is not accompanied by changes in depolarization ratio. The backscattering Ångstrom exponent $A^{\beta}_{355/532}$ is sensitive to the enhancement of dust absorption in UV and can be negative (Veselovskii et al., 2020a). For this episode $A^{\beta}_{355/532}$ decreases with height (together with G_F) to -0.3 at 2.5 km. Similar values of $A^{\beta}_{355/532}$ were observed during SHADOW campaign in Western Sahara (Veselovskii et al., 2020a). Above 3.75 km both $A^{\beta}_{355/532}$ and G_F start to increase. Hence, dust properties change with height and this change is not revealed on δ_{532} profile. We should mention, that in publication of Veselovskii et al. (2020a), increase of the dust imaginary part in UV also did not lead to changes in δ_{532}.

Application of our new "Fluorescence – Depolarization" based approach to six episodes considered in this section, demonstrates its ability to discriminate several aerosol types. The first step in validation of the results presented, could be comparison of the particle properties for obtained aerosol types with corresponding values, used in existing typing algorithms. Table 3 provides the range of variation of particle intensive properties from publications of Burton et al., (2013), synthetic values used in NATALI algorithm (Nicolae et al., 2018) and parameters used in the algorithm of Papagiannopoulos et al. (2018) for the urban, smoke and dust particles. The table contains also the range of properties variation for the episodes considered in current study for the same aerosol types. Parameters chosen in different algorithms, even for the same aerosol type, vary in a wide range, and the values observed in this study mainly match this range of variation. We observe higher values of $A^{\beta}_{355/532}$ for urban and smoke particles, and for dust, $A^{\beta}_{355/532}$ could be negative. Still, the values obtained in this study and the values used by other algorithms are in reasonable agreement.

Conclusion

The results presented in this study can be considered as the first important step in the combination of Mie – Raman and fluorescence lidar data. In approach presented, only two intensive parameters are used for classification: the particle depolarization ratio δ_{532} and the fluorescence capacity G_F. These parameters are chosen because they are specific for different types of aerosol and can be calculated with high spatio-temporal resolution. Moreover, δ_{532} and G_F can be calculated at lower altitudes, compared to extinction related parameters, such as lidar ratio and extinction Angstrom exponent. Thus classification, in principle, is possible at ranges with incomplete geometrical overlap. Finally, computation of β_F does not demand the use of reference height, only calibration of relative sensitivity of the channels is needed. Thus, aerosol classification is possible, even in the presence of low-level clouds.

Though only two aerosol properties are considered, the use of fluorescence provides advances in aerosol classification. Analysis of numerous observations, performed at Lille University for the period 2020 – 2021, demonstrates the possibility to separate four types of aerosols, such as dust, smoke, pollen and urban. Moreover, we are able to identify the layers containing the liquid water particles and ice. The number of determined aerosol classes can be increased, by considering the particle mixtures. In particular, "pure" dust can be considered separately from "polluted" one, which can be discriminated by lower values of the depolarization ratio.

Fluorescence technique is especially promising for separation of smoke and urban particles, because fluorescence capacity of smoke is about factor five higher. The important advantage of fluorescence measurements is the ability to identify the biological particles in the atmosphere, such as pollen, which are usually not included in the classification schemes, based on Mie-Raman observations. At the same time, our observations demonstrate that biological particles are frequently observed during Spring – Autumn seasons and may contribute significantly to the aerosol composition inside the PBL. The developed approach allows to identify aerosol types with high spatio-temporal resolutions, which is estimated to be 60 m for height and less than 10 minutes for time, for the current instrumental configuration. Such resolution provides an opportunity for investigating the dynamics of aerosol mixing in the troposphere.

The next step in algorithm development will be to include additional particle properties. We plan to include the backscattering Angstrom exponents and the depolarization spectral ratios ($\delta_{355}/\delta_{532}$ and $\delta_{532}/\delta_{1064}$), which can be also calculated with high spatio-temporal resolutions. The fluorescence capacity depends on the relative humidity, due to the effects of hygroscopic growth. Thus, information about spatio-temporal distribution of RH should be included in the analysis. It is also important to combine our algorithm with existing classification schemes, which we plan to consider in the near future.

Data availability. Lidar measurements are available upon request (philippe.goloub@univ-lille.fr).

Author contributions. IV processed the data and wrote the paper. QH and TP performed the measurements. PG supervised the project and helped with paper preparation. BB prepared algorithm for aerosol classification. MK developed software for data processing.

.

Competing interests. The authors declare that they have no conflict of interests.

Acknowledgement

We acknowledge funding from the CaPPA project funded by the ANR through the PIA under contract ANR-11-LABX-0005-01, the “Hauts de France” Regional Council (project CLIMIBIO) and the European Regional Development Fund (FEDER). ESA/QA4EO program is greatly acknowledged for support of observation activity at LOA as well as OBS4CLIM Equipex project funded by ANR. Development of algorithm for aerosol typing was supported by Russian Science

Foundation (project 21-17-00114). The SILAM model is acknowledged for providing pollen simulations.

References

Adam, M., Stachlewska, I. S., Mona, L., Papagiannopoulos, N., Bravo-Aranda, J. A., Sicard, M., Nicolae, D. N., Belegante, L., Janicka, L., Szczepanik, D., Mylonaki, M., Papanikolaou, C.-A., Siomos, N., Voudouri, K. A., Alados-Arboledas, L., Apituley, A., Mattis, I., Chaikovsky, A., Muñoz-Porcar, C., Pietruczuk, A., Bortoli, D., Baars, H., Grigorov, I., and Peshev, Z.: Biomass burning events measured by lidars in EARLINET – Part 2: Optical properties investigation, Atmos. Chem. Phys. Discuss., https://doi.org/10.5194/acp-2021-759, in review, 2021.

Ansmann, A., Riebesell, M., Wandinger, U., Weitkamp, C., Voss, E., Lahmann, W., and Michaelis, W.: Combined Raman elastic-backscatter lidar for vertical profiling of moisture, aerosols extinction, backscatter, and lidar ratio, Appl.Phys.B, *55*, 18-28, 1992.

Bohlmann, S., Shang, X., Giannakaki, E., Filioglou, M., Saarto, A., Romakkaniemi, S. and Komppula, M.: Detection and characterization of birch pollen in the atmosphere using multi-wavelength Raman lidar in Finland, Atmos. Chem. Phys. 19, 14559–14569, 2019. doi.org/10.5194/acp-19-14559-2019.

Boucher, O., Randall, D., Artaxo, P., Bretherton, C., Feingold, G., Forster, P., Kerminen, V.-M., Kondo, Y., Liao, H., Lohmann, U., Rasch, P., Satheesh, S. K., Sherwood, S., Stevens, B., and Zhang, X. Y.: Clouds and Aerosols, in: Climate Change 2013: The Physical Science Basis. Contribution of Working Group I to the Fifth Assessment Report of the Intergovernmental Panel on Climate Change, edited by: Stocker, T. F., Qin, D., Plattner, G.-K., Tignor, M., Allen, S. K., Boschung, J., Nauels, A., Xia, Y., Bex, V., and Midgley, P., M., Cambridge University Press, Cambridge, United Kingdom and New York, NY, USA, 2013

Burton, S. P., Ferrare, R. A., Hostetler, C. A., Hair, J.W., Rogers, R. R., Obland, M. D., Butler, C. F., Cook, A. L., Harper, D. B., and Froyd, K. D.: Aerosol classification using airborne High Spectral Resolution Lidar measurements – methodology and examples, Atmos. Meas. Tech., 5, 73–98, 2012. https://doi.org/10.5194/amt-5-73-2012

Burton, S. P., Ferrare, R. A., Vaughan, M. A., Omar, A. H., Rogers, R. R., Hostetler, C. A., and Hair, J. W.: Aerosol classification from airborne HSRL and comparisons with the CALIPSO vertical feature mask, Atmos. Meas. Tech., 6, 1397–1412, 2013. https://doi.org/10.5194/amt-6-1397-2013

Burton, S. P., Vaughan, M. A., Ferrare, R. A. and Hostetler, C. A.: Separating mixtures of aerosol types in airborne High Spectral Resolution Lidar data. Atmos. Meas. Tech. 7, 419-436, 2014. DOI: 10.5194/amt-7-419-2014

Burton, S. P., Hair, J. W., Kahnert, M., Ferrare, R. A., Hostetler, C. A., Cook, A. L., Harper, D. B., Berkoff, T. A., Seaman, S. T., Collins, J. E., Fenn, M. A., and Rogers, R. R.: Observations of the spectral dependence of linear particle depolarization ratio of aerosols using NASA Langley airborne High Spectral Resolution Lidar, Atmos. Chem. Phys., 15, 13453–13473, 2015 doi:10.5194/acp-15-13453-2015

Cao, X., Roy, G., and Bernier, R.: Lidar polarization discrimination of bioaerosols, Opt. Eng., 49, 116201, https://doi.org/10.1117/1.3505877, 2010.

Dubovik, O., Holben, B. N., Eck, T. F., Smirnov, A., Kaufman, Y. J., King, M. D., Tanre, D., and Slutsker, I.: Variability of absorption and optical properties of key aerosol types observed in worldwide locations, J. Atmos. Sci., 59, 590–608, 2002.

Freudenthaler,V., Esselborn, M.,Wiegner, M.,Heese, B., Tesche, M. and co-authors: Depolarization ratio profiling at several wavelengths in pure Saharan dust during SAMUM 2006, *Tellus* 61B, 165–179, 2009.

Gasteiger, J. and Freudenthaler, V.: Benefit of depolarization ratio at $\lambda = 1064$ nm for the retrieval of the aerosol microphysics from lidar measurements. Atmos. Meas. Tech. 7, 3773-3781, 2014. DOI: 10.5194/amt-7-3773-2014

Giles, D. M., Holben, B. N., Eck, T. F., Sinyuk, A., Smirnov, A., Slutsker, I., Dickerson, R. R., Thompson, A. M., and Schafer, J. S.: An analysis of AERONET aerosol absorption properties and classifications representative of aerosol source regions, J. Geophys. Res. 117, D17203, https://doi.org/10.1029/2012JD018127, 2012.

Groß, S., Tesche, M., Freudenthaler, V., Toledano, C., Wiegner, M., Ansmann, A., Althausen D., Seefeldner, M.:. Characterization of Saharan dust, marine aerosols and mixtures of biomass-burning aerosols and dust by means of multi-wavelength depolarization and Raman lidar measurements during SAMUM 2. Tellus B 63, 706-724, 2011. DOI: 10.1111/j.1600-0889.2011.00556.

Groß, S., Esselborn, M., Weinzierl, B., Wirth, M., Fix, A., and Petzold, A.: Aerosol classification by airborne high spectral resolution lidar observations, Atmos. Chem. Phys., 13, 2487–2505, 2013. https://doi.org/10.5194/acp-13-2487-2013

Haarig, M., Ansmann, A., Baars, H., Jimenez, C., Veselovskii, I., Engelmann, R., and Althausen, D.: Depolarization and lidar ratios at 355, 532, and 1064 nm and microphysical properties of aged tropospheric and stratospheric Canadian wildfire smoke, Atmospheric Chemistry and Physics, 18, 11 847–11 861, 2018.

Hamill, P., Giordano, M., Ward, C., Giles, D., and Holben, B.: An AERONET-based aerosol classification using the Mahalanobis distance, Atmos. Environ., 140, 213–233, https://doi.org/10.1016/j.atmosenv.2016.06.002, 2016.

Hara, Y., Nishizawa, T., Sugimoto , N., Osada, K., Yumimoto, K., Uno, I., Kudo, R., and Ishimoto, H.: Retrieval of aerosol components using multi-wavelength Mie-Raman lidar and comparison with ground aerosol sampling, Remote Sens., 10, 937, 2018. https://doi:10.3390/rs10060937

Hu, Q., Goloub, P., Veselovskii, I., Bravo-Aranda, J.-A., Popovici, I. E., Podvin, T., Haeffelin, M., Lopatin, A., Dubovik, O., Pietras, C., et al.: Long-range-transported Canadian smoke plumes in the lower stratosphere over northern France, Atmospheric Chemistry and Physics, 19, 1173–1193, 2019.

Hu, Q., Goloub, P., Veselovskii, I., and Podvin, T.: The characterization of long-range transported North American biomass burning plumes: what can a multi-wavelength Mie-Raman-polarization-fluorescence lidar provide?, Atmos. Chem. Phys., 22, 5399–5414, 2022 https://doi.org/10.5194/acp-22-5399-2022

HYSPLIT(2022): HYbrid Single-Particle Lagrangian Integrated Trajectory model, backward trajectory calculation tool, available at: http://ready.arl.noaa.gov/HYSPLIT_traj.php, last access: 14 June 2022.

Klett J.D., “Lidar inversion with variable backscatter/extinction ratios”, Appl.Opt. 24, 1638-1643, 1985.

Li, L., Dubovik, O., Derimian, Y., Schuster, G. L., Lapyonok, T., Litvinov, P., Ducos, F., Fuertes, D., Chen, C., Li, Z., Lopatin, A., Torres, B., and Che, H.: Retrieval of aerosol components directly from satellite and ground-based measurements, Atmos. Chem. Phys., 19, 13409–13443, 2019. https://doi.org/10.5194/acp-19-13409-2019

Mamouri, R.-E., and Ansmann, A.: Potential of polarization/Raman lidar to separate fine dust, coarse dust, maritime, and anthropogenic aerosol profiles, Atmos. Meas. Tech., 10, 3403–3427, 2017. https://doi.org/10.5194/amt-10-3403-2017

Müller, D., Mattis, I., Wandinger, U., Ansmann, A., Althausen, A., and Stohl, A.: Raman lidar observations of aged Siberian and Canadian forest fire smoke in the free troposphere over Germany in 2003: Microphysical particle characterization, J. Geophys. Res., 110, D17201, doi:10.1029/2004JD005756, 2005.

Mylonaki, M., Giannakaki, E., Papayannis, A., Papanikolaou, C.-A., Komppula, M., Nicolae, D., Papagiannopoulos, N., Amodeo, A., Baars, H., and Soupiona, O.: Aerosol type classification analysis using EARLINET multiwavelength and depolarization lidar observations, Atmos. Chem. Phys., 21, 2211–2227, 2021. https://doi.org/10.5194/acp-21-2211-2021

Nicolae, D., Vasilescu, J., Talianu, C., Binietoglou, I., Nicolae, V., Andrei, S., and Antonescu, B.: A neural network aerosol-typing algorithm based on lidar data, Atmos. Chem. Phys., 18, 14511–14537, 2018. https://doi.org/10.5194/acp-18-14511-2018

Papagiannopoulos, N., Mona, L., Amodeo, A., D'Amico, G., Gumà Claramunt, P., Pappalardo, G., Alados-Arboledas, L., Guerrero- Rascado, J. L., Amiridis, V., Kokkalis, P., Apituley, A., Baars, H., Schwarz, A.,Wandinger, U., Binietoglou, I., Nicolae, D., Bortoli, D., Comerón, A., Rodríguez-Gómez, A., Sicard, M., Papayannis, A., and Wiegner, M.: An automatic observation-based aerosol typing method for EARLINET, Atmos. Chem. Phys., 18, 15879– 15901, 2018. https://doi.org/10.5194/acp-18-15879-2018

Pappalardo, G., Amodeo, A., Apituley, A., Comeron, A., Freudenthaler, V., Linné, H., Ansmann, A., Bösenberg, J., D'Amico, G., Mattis, I., Mona, L., Wandinger, U., Amiridis, V., Alados-Arboledas, L., Nicolae, D., and Wiegner, M.: EARLINET: towards an advanced sustainable European aerosol lidar network, Atmos. Meas. Tech., 7, 2389–2409, 2014. https://doi.org/10.5194/amt- 7-2389-2014, 2014.

Reichardt, J., Leinweber, R., Schwebe, A.: Fluorescing aerosols and clouds: investigations of co-existence, Proceedings of the 28th ILRC, Bucharest, Romania, 25-30 June, 2017.

Rittmeister, F., Ansmann, A., Engelmann, R., Skupin, A., Baars, H., Kanitz, T., and Kinne, S.: Profiling of Saharan dust from the Caribbean to western Africa –Part 1: Layering structures and optical properties from shipborne polarization/Raman lidar observations, Atmos. Chem. Phys., 17, 12963–12983, 2017. https://doi.org/10.5194/acp-17-12963-2017

Saito,Y., Hosokawa, T., Shiraishi, K.: Collection of excitation-emission-matrix fluorescence of aerosol-candidate-substances and its application to fluorescence lidar monitoring, Appl. Opt., 61, 653 – 660, 2022.

Schuster, G. L., Dubovik, O., and Arola, A.: Remote sensing of soot carbon – Part 1: Distinguishing different absorbing aerosol species, Atmos. Chem. Phys., 16, 1565–1585, https://doi.org/10.5194/acp-16-1565-2016, 2016.

Sicard, M., Fortunato dos Santos Oliveira, D. C., Muñoz-Porcar, C., Gil-Díaz, C., Comerón, A., Rodríguez-Gómez, A., and Dios Otín, F.: Measurement Report: Spectral and statistical analysis of aerosol hygroscopic growth from multi-wavelength lidar measurements in Barcelona, Spain, Atmos. Chem. Phys. 22, 7681–7697, 2022. https://doi.org/10.5194/acp-22-7681-2022

Sofiev, M., Siljamo, P., Ranta, H., Linkosalo, T., Jaeger,S., Rasmussen, A., Rantio-Lehtimaki, A., Severova, E., Kukkonen, J. (2012) A numerical model of birch pollen emission and dispersion in the atmosphere. Description of the emission module. Int.J.Biometeorology, http://www.ncbi.nlm.nih.gov/pubmed/22410824, DOI 10.1007/s00484-012-0532-z, PMID 22410824

Sofiev, M., Vira, J., Kouznetsov, R., Prank, M., Soares, J., Genikhovich, E. (2015) Construction of the SILAM Eulerian atmospheric dispersion model based on the advection algorithm of Michael Galperin, Geosci.Model Developm. 8, 3497-3522, doi:10.5194/gmd-8-3497-2015

Sofiev, M. On impact of transport conditions on variability of the seasonal pollen index. Aerobiologia 33, 167–179 (2017). https://doi.org/10.1007/s10453-016-9459-x

Sugimoto, N. and Lee, C. H.: Characteristics of dust aerosols inferred from lidar depolarization measurements at two wavelengths. Applied Optics 45, 7468-7474, 2006. DOI: 10.1364/AO.45.007468

Sugimoto, N., Huang, Z., Nishizawa, T., Matsui, I., Tatarov, B.: Fluorescence from atmospheric aerosols observed with a multichannel lidar spectrometer," Opt. Expr. 20, 20800-20807, 2012.

Tesche, M., Ansmann, A., Müller, D., Althausen, D., Mattis, I., Heese, B., Freudenthaler, V., Wiegner, M., Eseelborn, M., Pisani, G., and Knippertz, P.: Vertical profiling of Saharan dust with Raman lidars and airborne HSRL in southern Morocco during SAMUM, Tellus B, 61, 144–164, 2009.

Veselovskii, I., Whiteman, D. N., Korenskiy, M., Suvorina, A., Perez-Ramirez, D.: Use of rotational Raman measurements in multiwavelength aerosol lidar for evaluation of particle backscattering and extinction, Atmos. Meas. Tech., 8, 4111–4122, 2015.

Veselovskii, I., Hu, Q., Goloub, P., Podvin, T., Korenskiy, M., Derimian, Y., Legrand, M., and Castellanos, P.: Variability in lidar-derived particle properties over West Africa due to changes in absorption: towards an understanding, Atmos. Chem. Phys., 20, 6563–6581, 2020a. https://doi.org/10.5194/acp-20-6563-2020a

Veselovskii, I., Hu, Q., Goloub, P., Podvin, T., Korenskiy, M., Pujol, O., Dubovik, O., Lopatin, A.: Combined use of Mie-Raman and fluorescence lidar observations for improving aerosol characterization: feasibility experiment, Atm. Meas. Tech., 13, 6691–6701, 2020b. doi.org/10.5194/amt-13-6691-2020.

Veselovskii, I., Hu, Q., Goloub, P., Podvin, T., Choël, M., Visez, N., and Korenskiy, M.: Mie–Raman–fluorescence lidar observations of aerosols during pollen season in the north of France, Atm. Meas. Tech., 14, 4773–4786, 2021. doi.org/10.5194/amt-14-4773-2021

Veselovskii, I., Hu, Q., Ansmann, A., Goloub, P., Podvin, T., Korenskiy, N.: Fluorescence lidar observations of wildfire smoke inside cirrus: A contribution to smoke-cirrus - interaction research, Atmos. Chem. Phys. 22, 5209–5221, 2022. https://doi.org/10.5194/acp-22-5209-2022

Voudouri, K. A., Siomos, N., Michailidis, K., Papagiannopoulos, N., Mona, L., Cornacchia, C., Nicolae, D., and Balis, D.: Comparison of two automated aerosol typing methods and their application to an EARLINET station, Atmos. Chem. Phys., 19, 10961–10980, 2019. https://doi.org/10.5194/acp-19-10961-2019

Wang, N., Shen, X., Xiao, D., Veselovskii, I., Zhao,C., Chen, F., Liu, C., Rong, Y., Ke, J., Wang, B., Qi, B., Liu, D.: Development of ZJU high-spectral-resolution lidar for aerosol and cloud: feature detection and classification, Journal of Quantitative Spectroscopy & Radiative Transfer, v.261, 107513, 2021. doi.org/10.1016/j.jqsrt.2021.107513

Whiteman, D.N.: Examination of the traditional Raman lidar technique. II. Evaluating the ratios for water vapor and aerosols, Appl. Opt., 42, 2593-2608, 2003. https://doi.org/10.1364/AO.42.002593

Zhang, Y., Li, Z., Chen, Y., Leeuw, G., Zhang, C., Xie, Y., and Li, K.: Improved inversion of aerosol components in the atmospheric column from remote sensing data, Atmos. Chem. Phys., 20, 12795–12811, 2020. https://doi.org/10.5194/acp-20-12795-2020

Zhang, Y., Sun, Z., Chen, S., Chen, H., Guo, P., Chen, S., He, J., Wang, J., Nian, X.: Classification and source analysis of low-altitude aerosols in Beijing using fluorescence–Mie polarization lidar, Optics Communications, 479, 126417, 2021. https://doi.org/10.1016/j.optcom.2020.126417

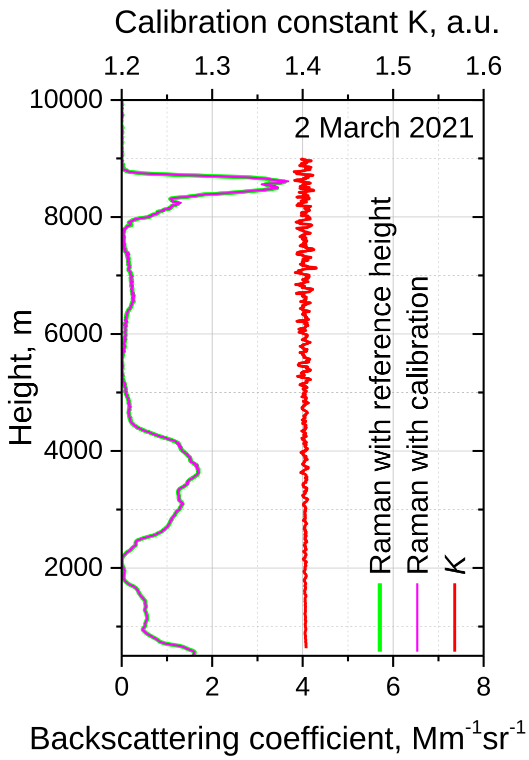

Fig.1. Backscattering coefficients at 532 nm for period 19:00 – 20:00 UTC on 2 March 2021 calculated from Mie-Raman observations using the reference height as Ansmann et al. (1992) (green) or the calibration constant as in Eq 5. (magenta). The profile of calibration constant *K* is shown with red line.

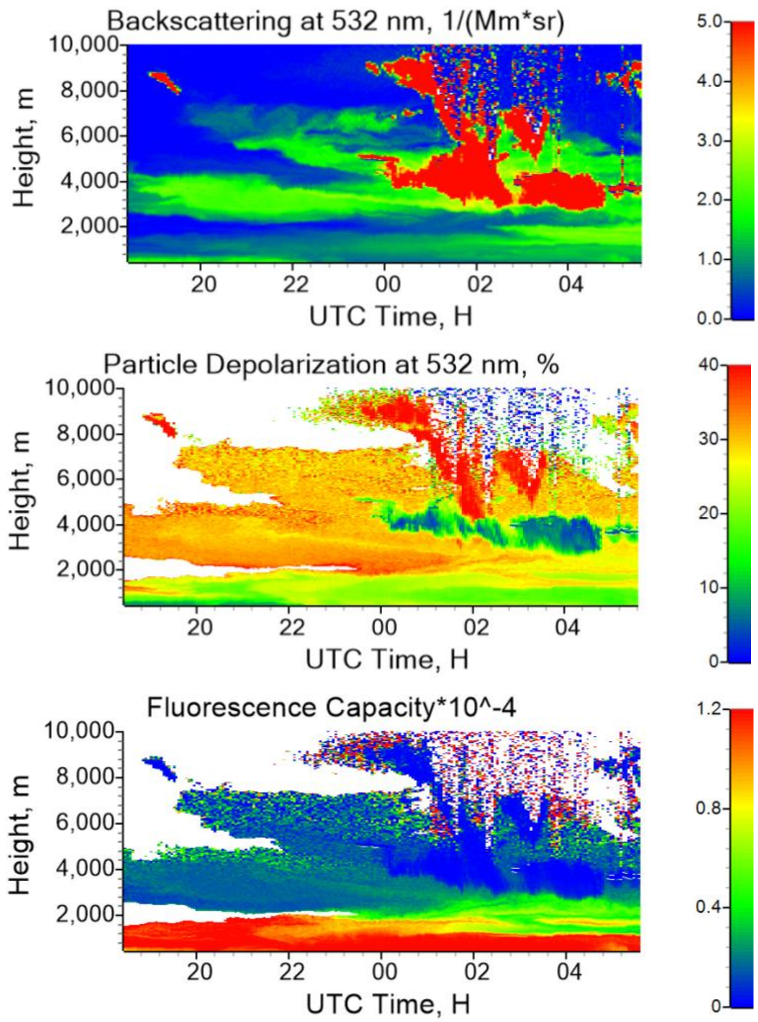

Fig.2. Spatio-temporal distributions of the backscattering coefficient β_{532}, the particle depolarization ratio δ_{532} and the fluorescence capacity G_F in the night 2-3 March 2021. The backscattering coefficient β_{532} is calculated with the modified Raman method. The values of δ_{532}, and G_F are shown for β_{532}>0.2 $Mm^{-1}sr^{-1}$.

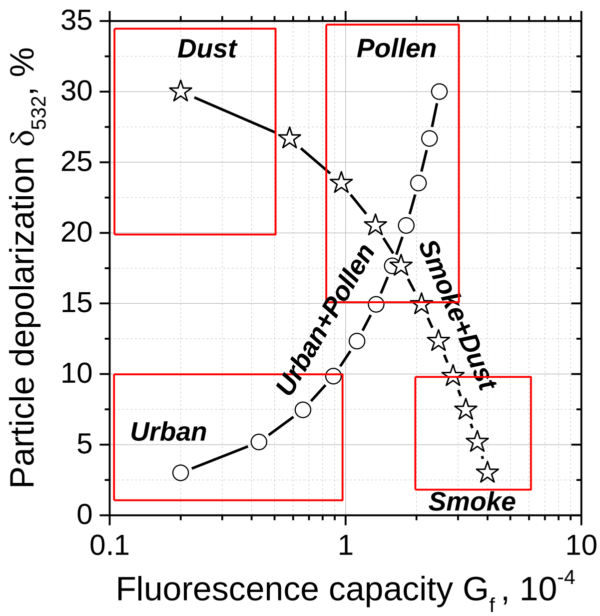

Fig.3. Aerosol typing with δ_{532}-G_F diagram. The ranges of the particle parameters variation for dust, pollen, smoke and urban aerosol are given by rectangles. The symbols show the results of simulation performed for pollen+urban (circles) and smoke + dust (stars) mixtures. Relative contribution of pollen (smoke) to the total backscattering β_{532} varied in 0 – 1.0 range with step 0.1. Particle parameters used in calculations are given in the text.

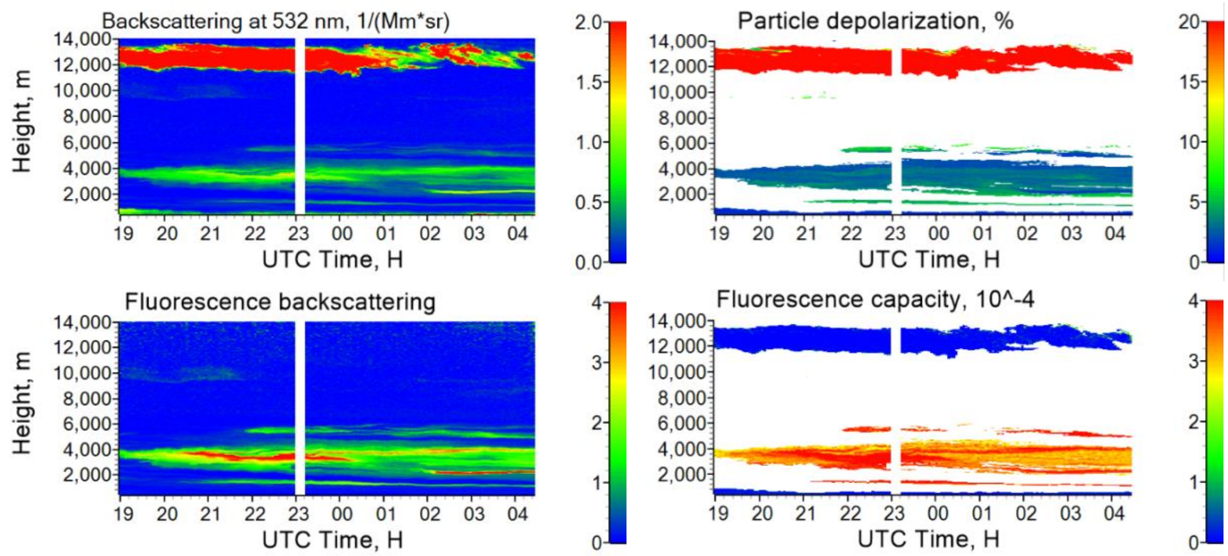

Fig.4. Spatio-temporal distributions of the backscattering coefficient β_{532}, the fluorescence backscattering coefficient β_F (in 10^{-4} $Mm^{-1}sr^{-1}$), the particle depolarization ratio δ_{532}; and the fluorescence capacity G_F in the night 12-13 September 2020. Calculation of δ_{532} and G_F was not performed for β_{532}<0.2 $Mm^{-1}sr^{-1}$.

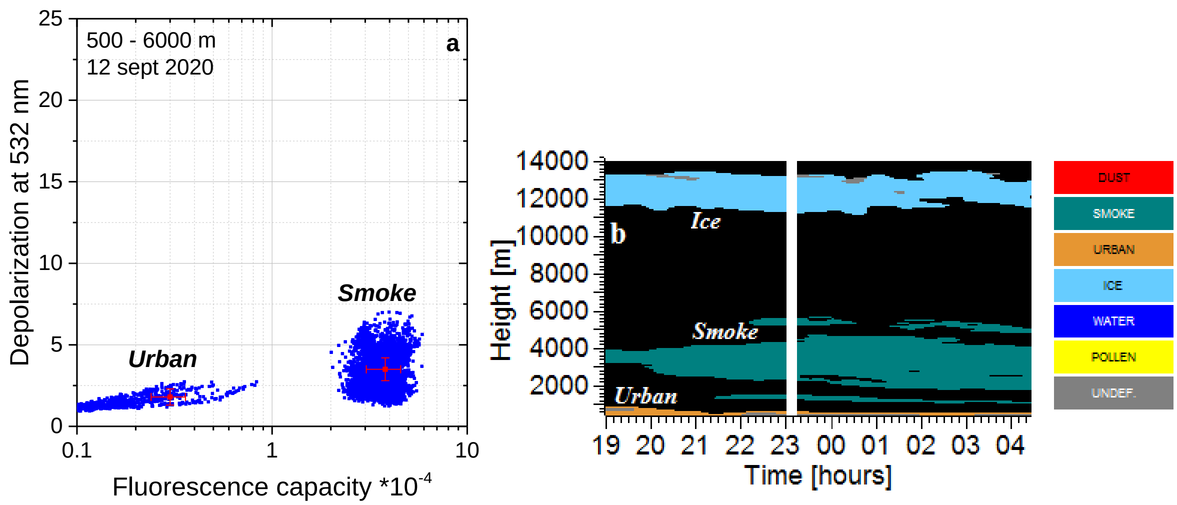

Fig.5 (a) The δ_{532}-G_F diagram for data from Fig.4 in 500 – 6000 m height range, red crosses show the uncertainty of the measurements. (b) Spatio-temporal distribution of aerosol types in the night 12-13 September 2020. Grey color shows undefined aerosol type, while measurements with β_{532}<0.2 $Mm^{-1}sr^{-1}$ are marked by black color.

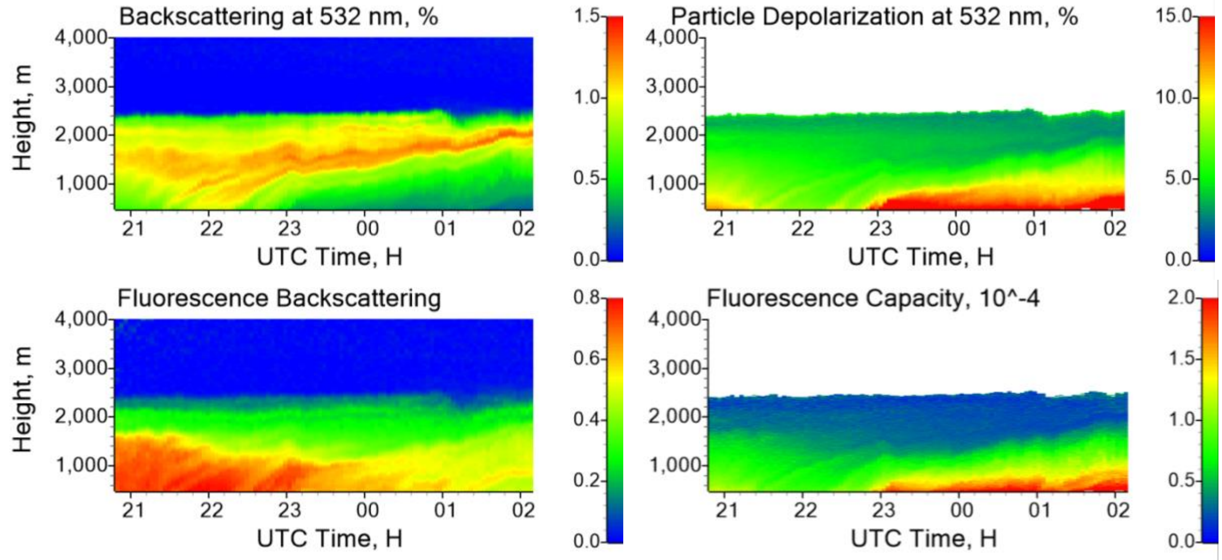

Fig.6. Spatio-temporal distributions of the backscattering coefficient β_{532}; the fluorescence backscattering coefficient β_F (in 10^{-4} $Mm^{-1}sr^{-1}$); the particle depolarization ratio δ_{532}; and the fluorescence capacity G_F in the night 30-31 May 2020.

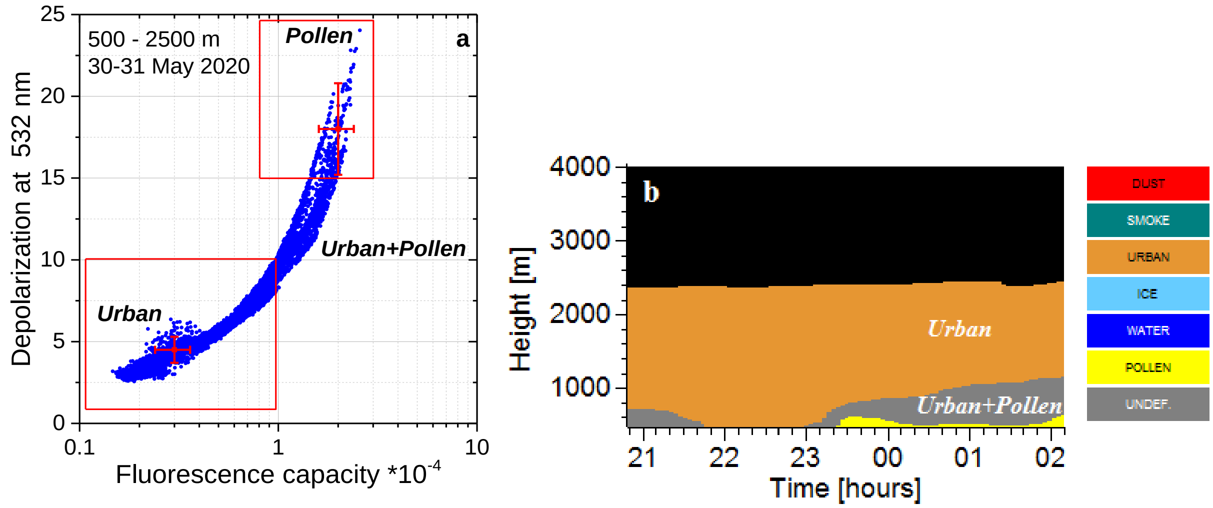

Fig.7. (a) The δ_{532}-G_F diagram for observations in 500 m – 2500 m height range and (b) spatio-temporal distribution of aerosol types on the night 30-31 May 2020. Grey color shows undefined aerosol type, which is a mixture of urban and pollen for this case. Measurements with β_{532}<0.2 $Mm^{-1}sr^{-1}$ are marked by black color.

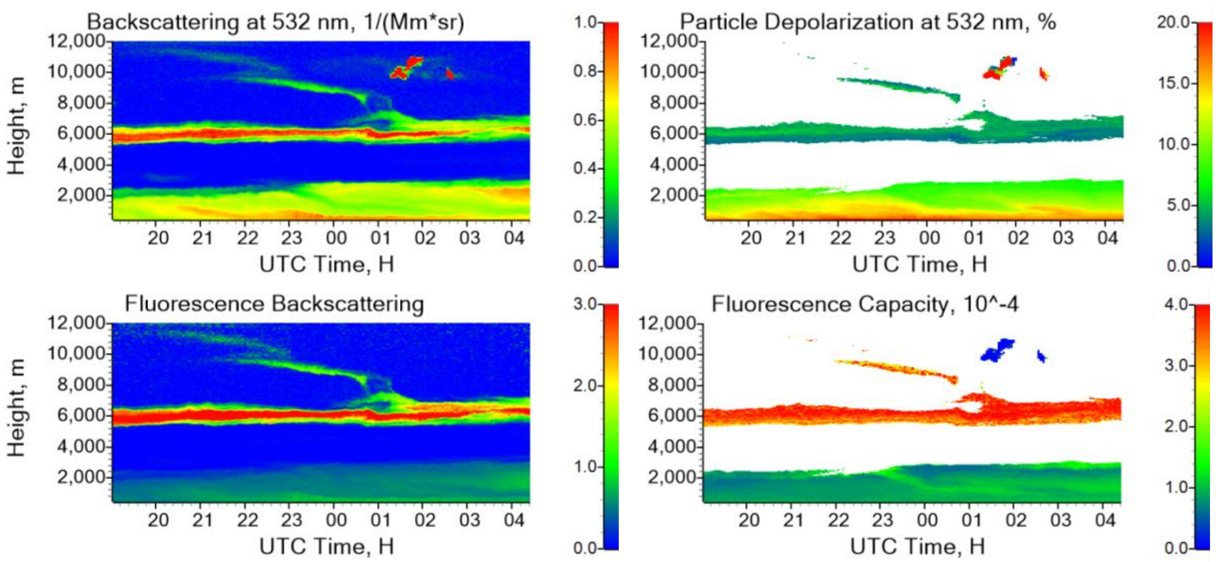

Fig.8. Spatio-temporal distributions of the backscattering coefficient β_{532}, the fluorescence backscattering coefficient β_F (in 10^{-4} $Mm^{-1}sr^{-1}$), the particle depolarization ratio δ_{532}, and the fluorescence capacity G_F in the night 14 – 15 September 2020. Measurements with β_{532}<0.2 $Mm^{-1}sr^{-1}$ are marked by black color.

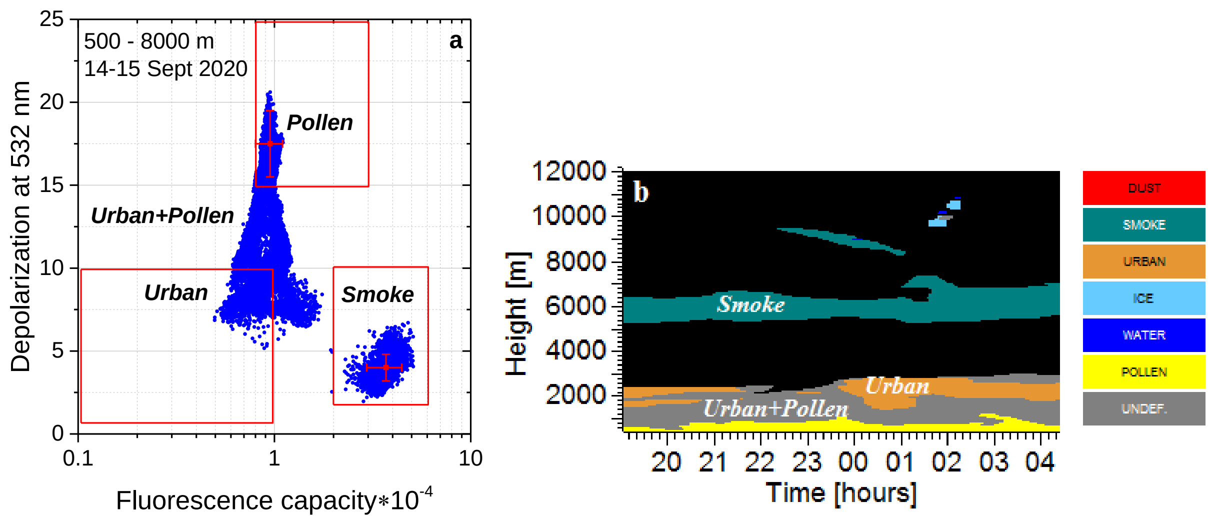

Fig.9. (a) The δ_{532}-G_F diagram for observations in 500 m – 8000 m height range and (b) spatio-temporal distribution of aerosol types in the night 14 – 15 September 2020. Grey color shows undefined aerosol type, which is a mixture of pollen, urban and smoke particles.

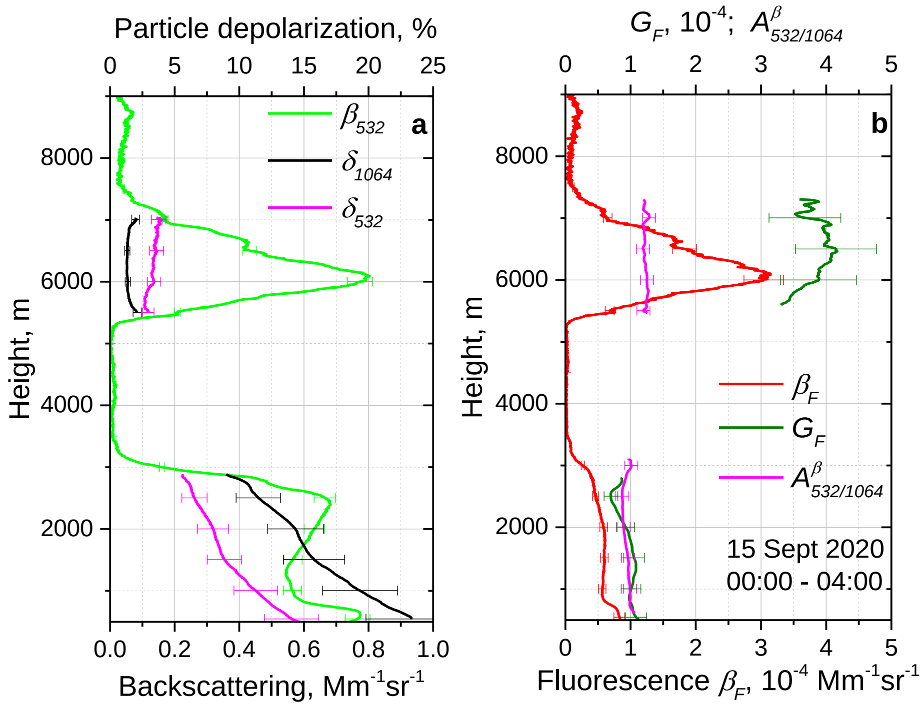

Fig.10. Vertical profiles of (a) backscattering coefficient β_{532} and particle depolarization ratios δ_{532}, δ_{1064}; (b) fluorescence backscattering β_F, fluorescence capacity G_F and backscattering Angstrom exponent $A^{\beta}_{532/1064}$ on 15 September 2020 for period 00:00 – 04:00 UTC.

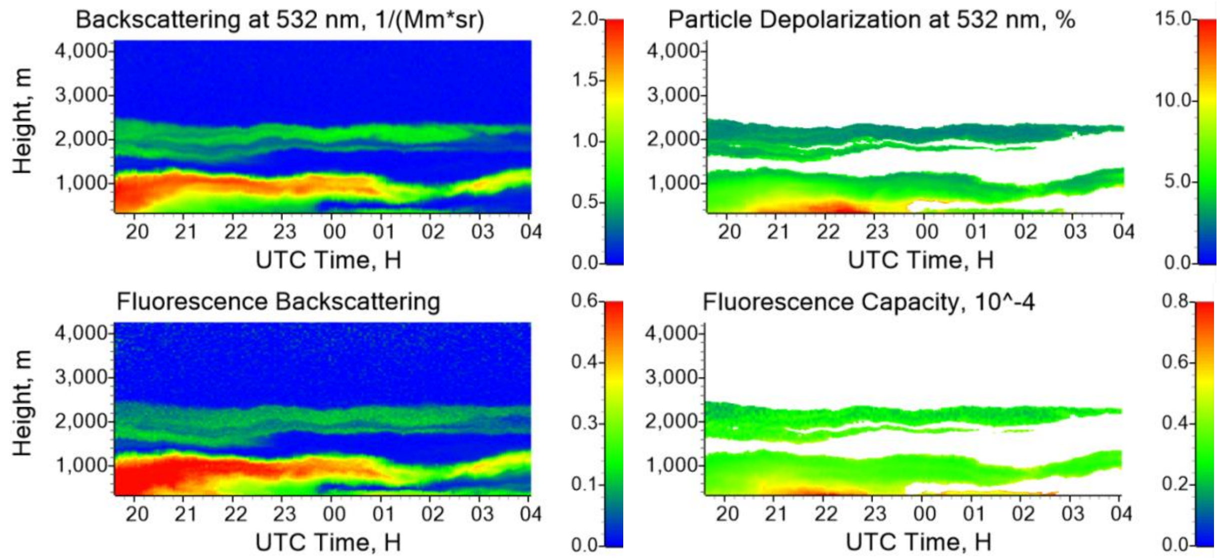

Fig.11. Spatio-temporal distributions of the backscattering coefficient β_{532}, the fluorescence backscattering coefficient β_F (in 10^{-4} $Mm^{-1}sr^{-1}$), the particle depolarization ratio δ_{532}; and the fluorescence capacity G_F in the night 10 – 11 April 2020. Measurements are performed at an angle of 45 dg to horizon.

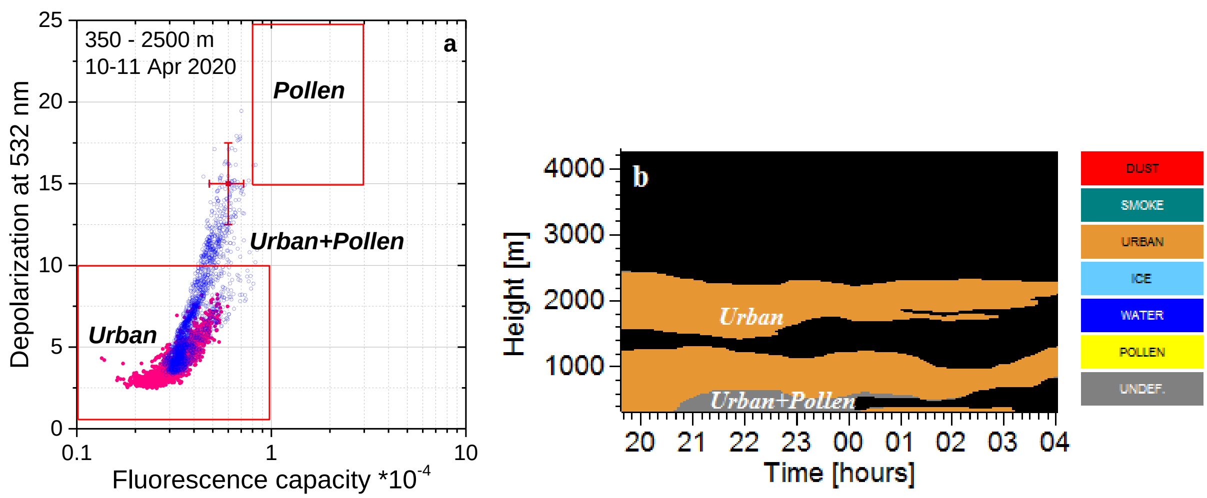

Fig.12. (a) The δ_{532}-G_F diagram for observations in 350 – 1500 m (blue symbols) and 1500 – 2500 m (pink symbols) height ranges. (b) Spatio-temporal distribution of aerosol types in the night 10 – 11 April 2020. Grey color shows undefined aerosol type, which is a mixture of urban and pollen for this case. Measurements with β_{532}<0.2 $Mm^{-1}sr^{-1}$ are marked by black color.

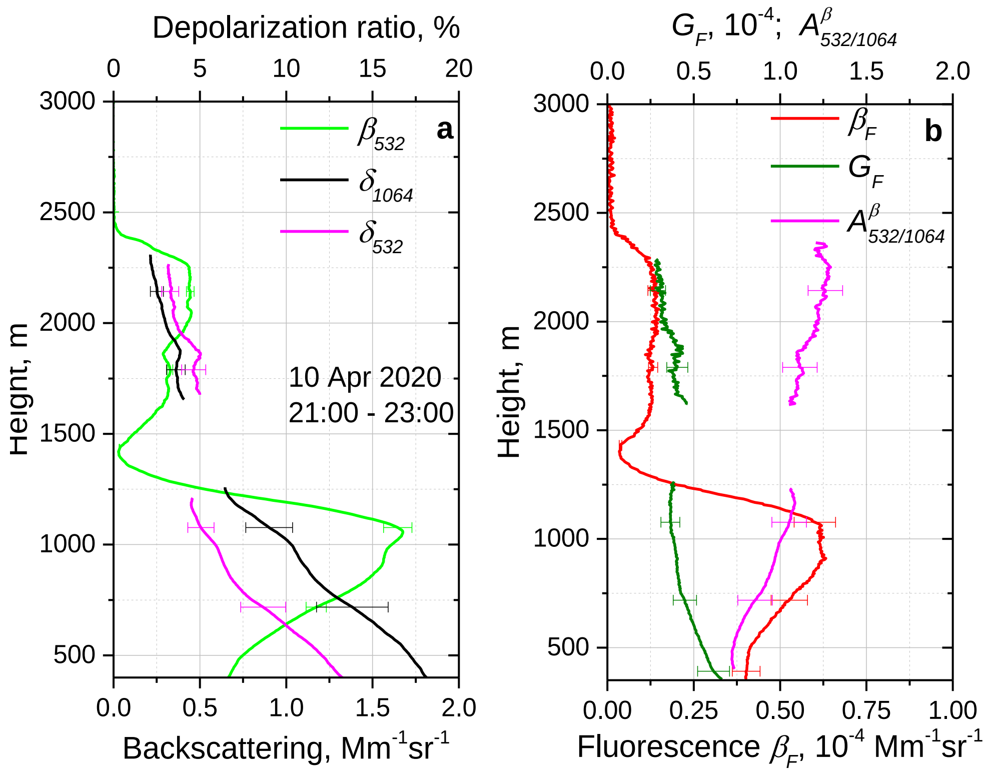

869

870 Fig.13. Vertical profiles of (a) backscattering coefficient β_{532} and particle depolarization ratios δ_{532},

871 δ_{1064}; (b) fluorescence backscattering β_F, fluorescence capacity G_F and backscattering Angstrom

872 exponent $A^{\beta}_{532/1064}$ on 10 April 2020 for period 21:00 – 23:00 UTC.

873

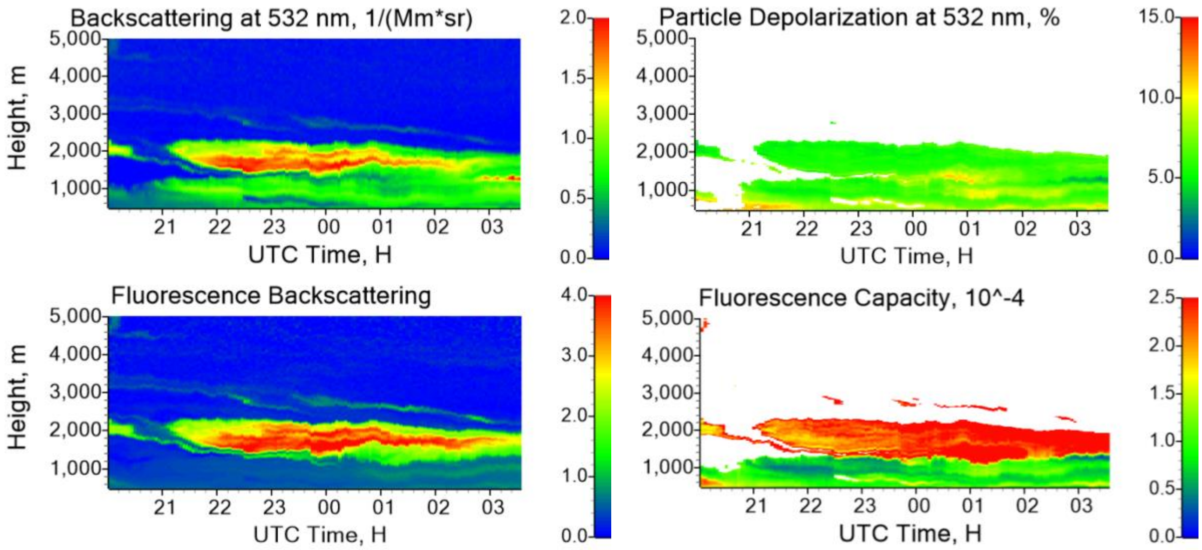

Fig.14. Spatio-temporal distributions of the backscattering coefficient β_{532}, the fluorescence backscattering coefficient β_F (in 10^{-4} $Mm^{-1}sr^{-1}$), the particle depolarization ratio δ_{532}, and the fluorescence capacity G_F in the night 11 – 12 August 2021. Measurements with β_{532}<0.2 $Mm^{-1}sr^{-1}$ are marked by black color.

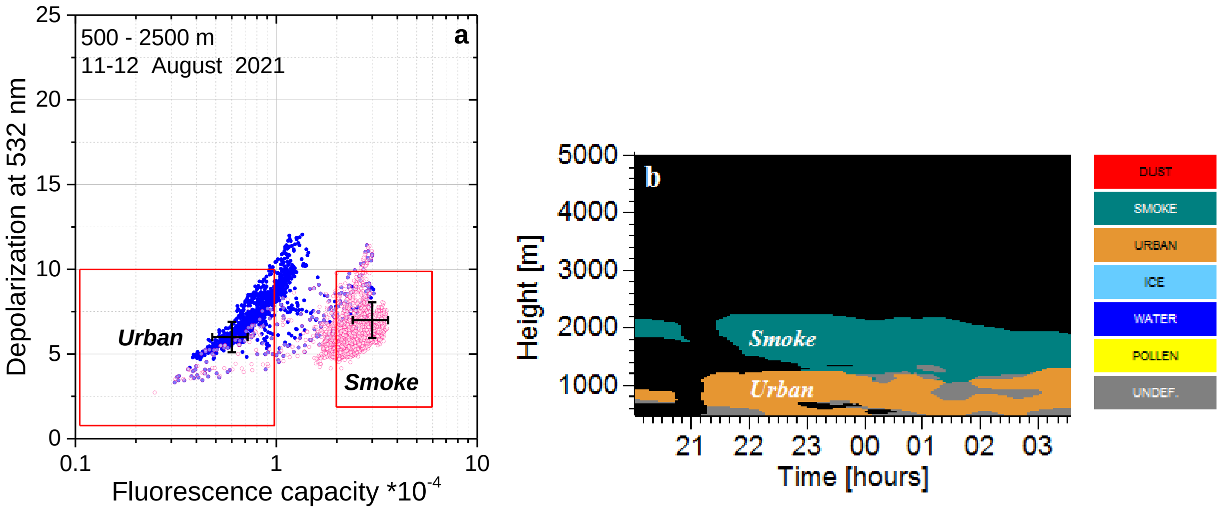

Fig.15. (a) The δ_{532}-G_F diagram for observations in 500 – 1400 m (blue symbols) and 1400 – 2500 m (pink symbols) height ranges. (b) Spatio-temporal distribution of aerosol types in the night 11-12 August 2021.

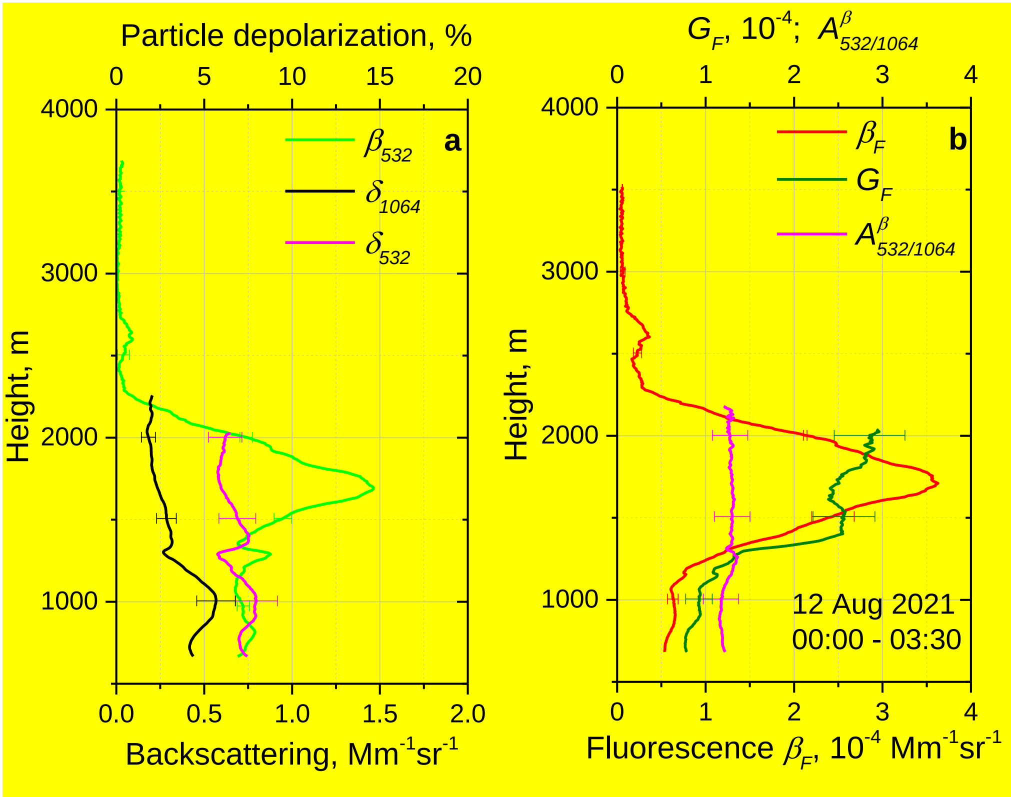

Fig.16. Vertical profiles of (a) backscattering coefficient β_{532} and particle depolarization ratios δ_{532}, δ_{1064}; (b) fluorescence backscattering β_F, fluorescence capacity G_F and backscattering Angstrom exponent $A^{\beta}_{532/1064}$ on 12 August 2021 for period 00:00 – 03:30 UTC.

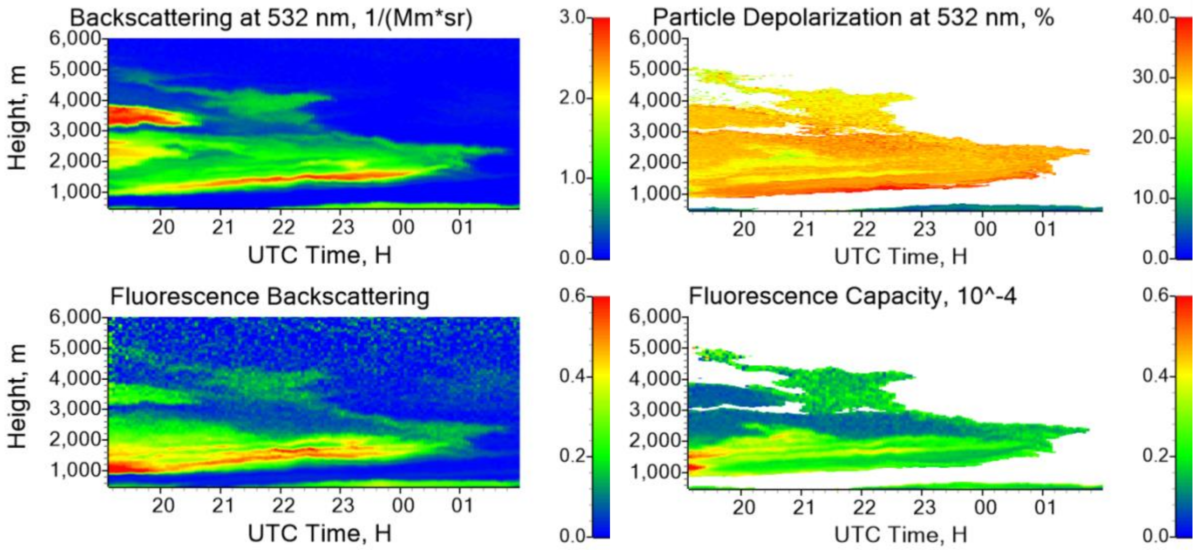

Fig.17. Height – temporal distributions of the backscattering coefficient at 532 nm β_{532}, the fluorescence backscattering coefficient β_F (in 10^{-4} $Mm^{-1}sr^{-1}$), the particle depolarization ratio at 532 nm δ_{532}, and the fluorescence capacity G_F in the night 1-2 April 2021.

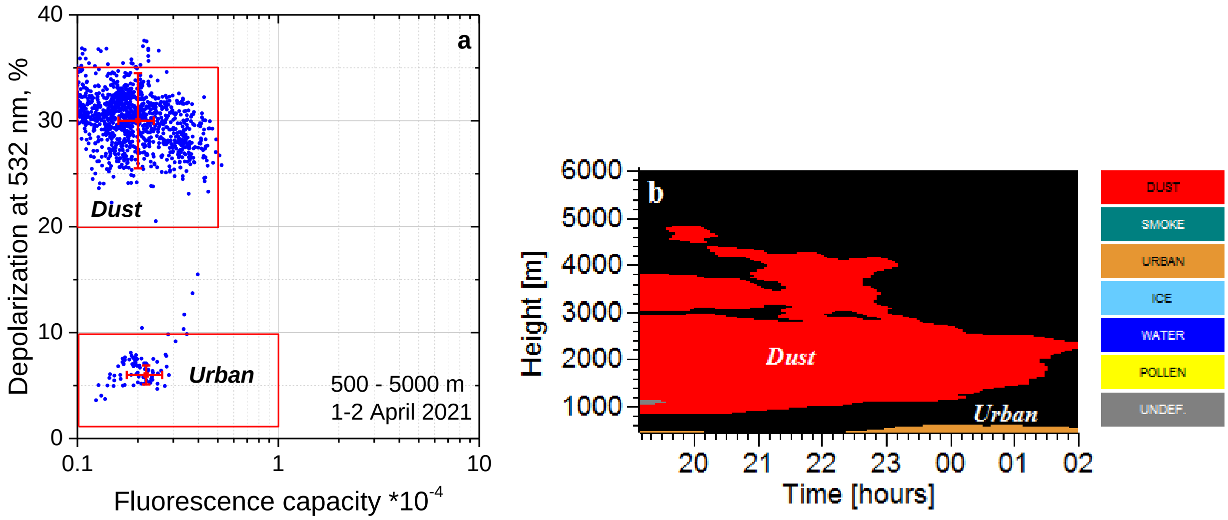

Fig.18. (a) The δ_{532}-G_F diagram for observations in 500 – 5000 m height range and (b) spatio-temporal distribution of aerosol types in the night 1-2 April 2021.

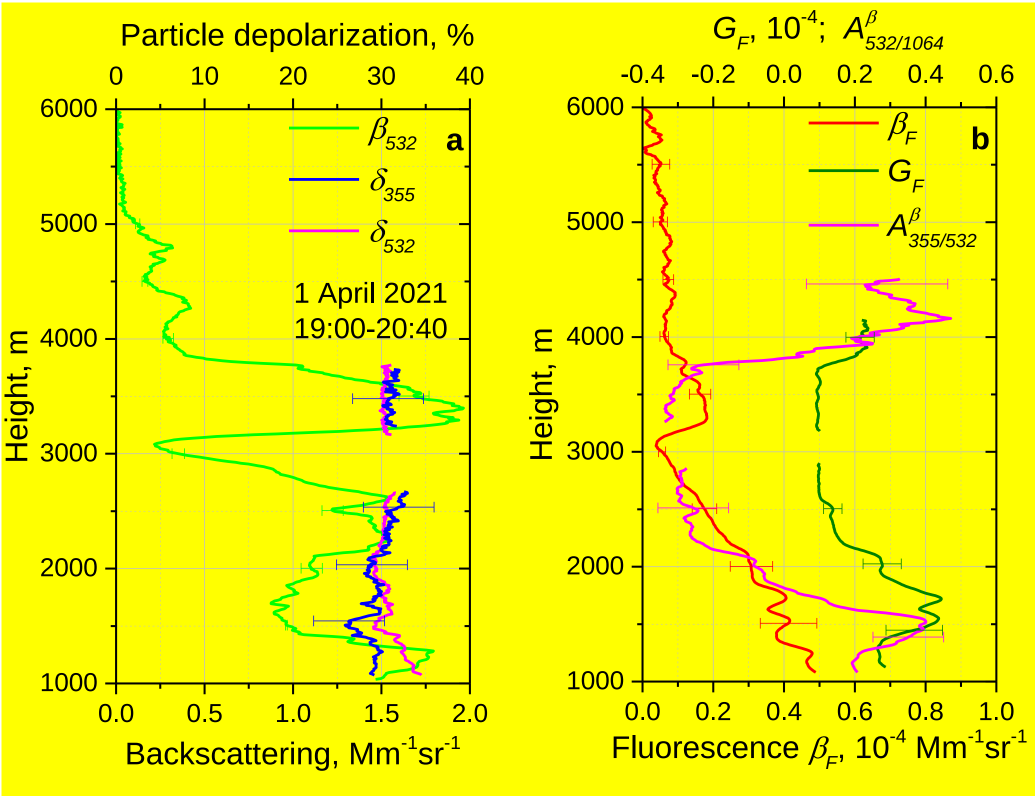

Fig.19. Vertical profiles of (a) backscattering coefficient β_{532} and particle depolarization ratios δ_{532}, δ_{355}; (b) fluorescence backscattering β_F, fluorescence capacity G_F and backscattering Angstrom exponent $A^{\beta}_{355/532}$ on 1 April 2021 for period 19:00 – 20:40 UTC.

Table 1. Ranges of particle depolarization δ_{532} and fluorescence capacity G_F, which were used for aerosol classification.

Aerosol type	δ_{532}, %	G_F, ($\times 10^{-4}$)
Dust	20 - 35	0.1 – 0.5
Pollen	15 - 35	0.8 – 3.0
Urban	1 - 10	0.1 – 1.0
Smoke	2- 10	2.0 – 6.0
Ice	>40	<0.01
Water	<5	<0.01

Table 2. Intensive particle parameters such as the lidar ratios (S_{355}, S_{532}), particle depolarization ratios (δ_{355}, δ_{532}, δ_{1064}), extinction ($A^{\alpha}_{355/532}$) and backscattering ($A^{\beta}_{355/532}$, $A^{\beta}_{532/1064}$) Angstrom exponents for six episodes, analyzed in this work. Parameters are given for chosen height – temporal intervals and the types of aerosol are determined from fluorescence measurements.

Date	Time, UTC	H, km	Type	S_{355}, sr	S_{532}, sr	δ_{355}, %	δ_{532}, %	δ_{1064}, %	$A^{\alpha}_{355/532}$	$A^{\beta}_{355/532}$	$A^{\beta}_{532/1064}$
10.04.2020	21:00-23:00	0.9-1.1 2.0-2.2	Urb.+Poll. Urban	48±7 50±7	48±7 70±10	5.0±1.0 7.0±1.0	6.0±1.0 3.5±0.7	10±1.5 3.0±0.6	1.3±0.2 1.1±0.2	1.4±0.2 2.0±0.2	1.0±0.2 1.2±0.2
30.05.2020	21:00-02:00	1.8-2.0	Urban	60±9	55±8	3.6±0.8	4.0±0.8	5.7±1.0	2.0±0.2	1.6±0.2	1.2±0.2
12.09.2020	20:00-23:00	3.2-3.8	Smoke	50±7	80±12	4.5±1.0	3.0±0.6	2.0±0.4	1.0±0.2	2.2±0.2	1.2±0.2
15.09.2020	00:00-04:00	1.4-1.6 5.8-6.2	Pollen Smoke	40±6 45±7	37±6 70±10	9.5±1.5 9.0±1.5	8.0±1.5 3.5±0.7	15±2.5 1.4±0.3	1.6±0.2 0.8±0.2	1.4±0.2 2.0±0.2	0.9±0.2 1.2±0.2
01.04.2021	19:00-20:40	2.25-2.5	Dust	57±8	52±8	30±4.5	30±4.5	-	0±0.2	-0.3±0.2	-
11.08.2021	22:00-24:00	1.0-1.2 1.5-2.0	Urban Smoke	42±7 45±7	55±8 72±11	- -	8.0±1.2 6.0±0.9	5.7±0.8 2.5±0.5	1.3±0.2 1.0±0.2	1.5±0.2 2.2±0.2	1.1±0.2 1.2±0.2

Table 3. Intensive particle parameters from publications of Burton et al., (2013); Nicolae et al., (2018); and Papagiannopoulos et al., (2018) together with values observed in current study for the urban, smoke and dust particles.

	Burton et al., 2013	Nicolae et al., 2018	Papagiannopoulos et al., 2018	This study
	Urban	Continental (rural)	Clear continental	Urban
S_{355}, sr		43-54	50±8	42 - 60
S_{532}, sr	43-81	52-53	41±6	55 -70
$A^{\alpha}_{355/532}$	-	1.2-1.3	1.7±0.6	1.1 -2.0
$A^{\beta}_{355/532}$	-	1.0-1.6	1.3±0.3	1.5 - 2.0
$A^{\beta}_{532/1064}$	0.49-1.3	0.54 – 1.0	1.0±0.3	1.1 - 1.2
Smoke				
S_{355}, sr	-	56-72	81±16	40 - 50
S_{532}, sr	46-87	81-92	78±11	70 - 80
$A^{\alpha}_{355/532}$	-	1.1-1.3	1.3±0.3	0.8 - 1.0
$A^{\beta}_{355/532}$	-	1.4 -2.1	1.2±0.3	2.0 - 2.4
$A^{\beta}_{532/1064}$	0.48-1.6	0.7-0.8	1.3±0.1	1.2
Dust				
S_{355}, sr	-	43-46	58±12	57
S_{532}, sr	41-57	44-49	55±7	52
$A^{\alpha}_{355/532}$	-	0.88-0.92	0.3±0.4	0
$A^{\beta}_{355/532}$	-	0.91-0.97	0.3±0.2	-0.3
$A^{\beta}_{532/1064}$	0.49-0.68	0.16-0.22	0.4±0.1	-

Appendix. Pollen index provided by SILAM

The SILAM is a chemical transport model, developed by the Finnish Meteorological Institute (Sofiev et al., 2015). It provides information on atmospheric composition, air quality, and pollen. In the pollen module of SILAM, six pollen types (alder, birch, grass, mugwort, olive, ragweed) are considered. The pollen index is defined as a quantitative measure of the severity of the pollen season and a proxy of the allergenic exposure (Sofiev et al., 2012, 2017). This higher the pollen index is, the more pollen grains in the atmosphere and the higher allergy risk. Fig. A1 shows the maps of pollen index in 4 cases. According to the description of SILAM model, the pollen index is labeled as "very high", when its value is greater than 4.0.

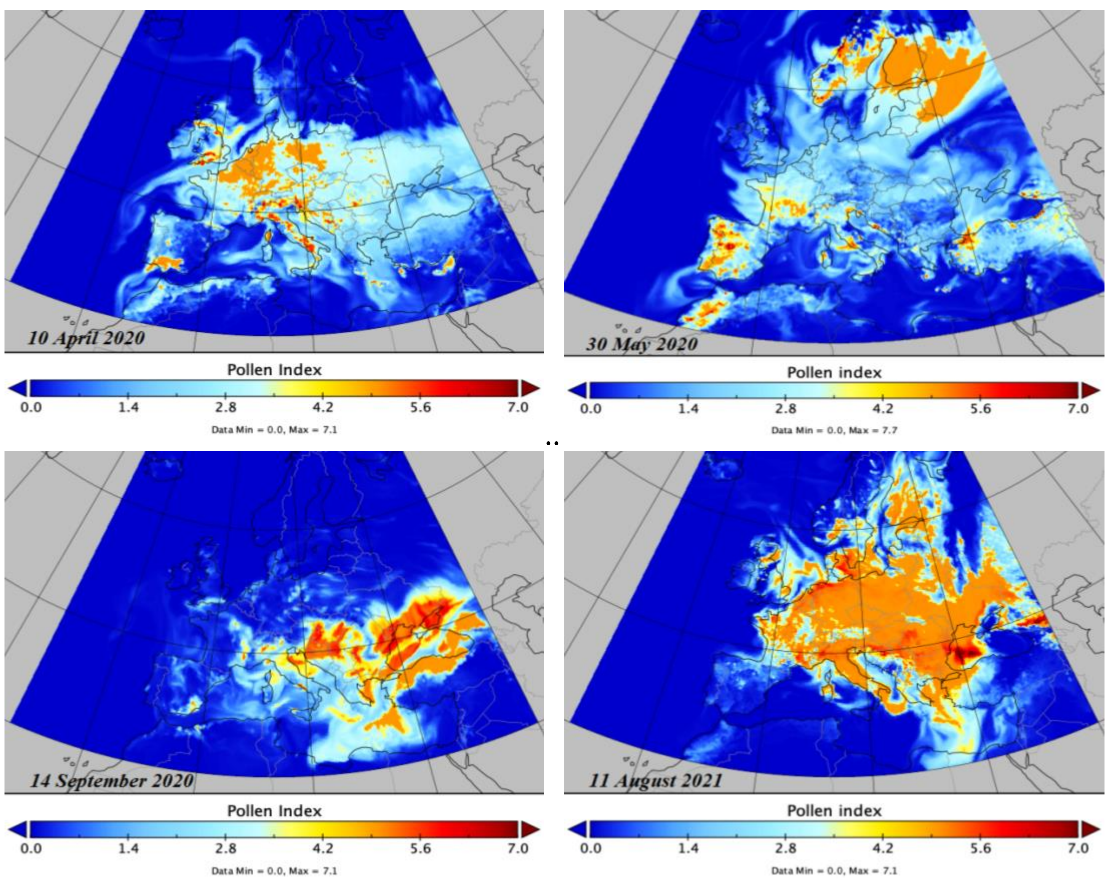

Fig.A1. Pollen index provided by SILAM for 10 April 2020, 30 May 2020, 14 September 2020 and 11 August 2021. The levels of pollen index are – very low (<1.0), low (<2.0), moderate (<3.0), high (< 4.0) and very high (>=4.0).

First of all we would like to thank the reviewer for very detailed comments and useful suggestions, which helped us to improve the revised manuscript

The manuscript describes several case studies of lidar observations where fluorescence observations combined with lidar depolarization shows significantly different properties for pollen, smoke, dust and anthropogenic aerosol. I'm excited to see the potential of these new measurements, which give completely independent and orthogonal information about aerosol particles, at single bin resolutions, significantly increasing the information available for aerosol typing. The case studies are a nice selection of different types and mixtures and interesting to see.

The manuscript seems to suffer from an identity problem, however. Mostly it is an illustrative set of cases studies that demonstrate differences in the two-dimensional space of fluorescence capacity and particle depolarization. It includes nice analysis of some mixtures of types as well. However, the paper claims to be an algorithm description paper, and for that purpose, analysis of a few hand-selected case studies really isn't sufficient, and the mixture analysis doesn't exactly fit, because it is not part of the algorithm. Apparently in consequence of this uncertainty about the desired focus of the paper, some aspects of the paper seem superficial, or rather, inconsistent in depth. The inferences in the paper about the types seem very reasonable, but many are not backed up by any independent information or compared with other methods of classification, which should be done to demonstrate the validity of the new algorithm, particularly if this is the algorithm description paper. Also there's insufficient information about how the thresholds in the algorithm were chosen. In the analysis of the case studies, there should be a consistent effort to include complimentary information to validate the case identifications using other measurements (in situ or other lidar measurements that reveal type) and backtrajectories. And if a major focus of the paper is to showcase the performance of a new (and better) classification algorithm, then the results should be shown on a bulk of data in addition to the case studies, and comparisons with other classification methods should be made and discussed.

The goal of this manuscript is to demonstrate that the fluorescence – depolarization diagram allows to separate different types of aerosol and provides new independent information on aerosol type, which can be used in classification schemes. The reviewer is right, at current stage of research it is not appropriate to call it “algorithm”, so we escape this term in the revised manuscript.
In the revised manuscript we tried to follow the reviewer recommendations. We added a table, containing the particle intensive parameters for the cases considered (lidar ratios at 355 and 532 nm; depolarization ratios at 355, 532 and 1064 nm; and the backscattering and extinction Angstrom exponents). Another table provides the range of variation of particle intensive properties from different typing algorithms for the urban, smoke and dust particles. The table contains also the range of parameters variation for episodes from current study for the same aerosol types.
The back-trajectory analysis is included.
In Appendix we added four maps with SILAM pollen index, for the episodes where the presence of the pollen was revealed. We hope, that all this improved the manuscript.

Specific comments:

L24. "and their mixtures". The mixture analysis is an interesting part of the paper, and apparently new compared to the authors' other papers, but it appears it's not really part of the classification algorithm, in the sense that mixture analysis can only be done on a case-by-case basis. Any discussion about that? This could be clarified in the abstract. Also, the mixture analysis is not even mentioned in the introduction. Discussing it there would help to clarify the novel aspects of the paper.

The mixture analysis is an important but in the manuscript presented we just identify the main mixture components, based on the patterns in depolarization – fluorescence diagram. Quantification of the mixture composition is the next step in our research and corresponding algorithm is in preparation at the moment. We removed from Abstract the mentioning of mixture analysis.

L73-75. I very much agree that adding independent aerosol information will improve classification, but this specific point is unconvincing. Yes, the variables used for classification so far have variability within types but there's nothing to suggest that this won't also be true for fluorescence capacity, is there? So, I'm not sure this is exactly the right motivation.

The advantage of fluorescence is strong variation of fluorescence capacity between some aerosol types. For example, G_F of smoke can up to one order higher, comparing to urban aerosol, allowing to separate these particles. So we think, that synergy of existing algorithms with fluorescence measurements should improve identification. Another important advantage is that G_F and depolarization can be derived with high spatio – temporal resolution, so almost single pixel typing becomes possible.

L105. Good point that the resolution is higher since fluorescence capacity can be calculated using data at a single bin, unlike extinction or other quantities related to extinction. This seems particularly useful for Raman measurements.

Yes.

L105-107. Veselovskii et al. 2021a is referenced extensively in the introduction, including to say that it already demonstrates the ability of the 2-d measurement space to separate all the aerosol types. I couldn't follow how the purpose and scope of this paper is different from 2021a.

In that paper we just formulated the idea and plotted averaged data for several observations on the depolarization – fluorescence diagram. In this manuscript we evaluate the aerosol type mask with almost singe pixel resolution. Corresponding paragraph is added to the revised manuscript.

L183-193. Calculation of the backscatter coefficient using a calibration constant sounds so straightforward, that I didn't realize that it hadn't been done before. This is great. It's good to see a relatively straightforward innovation discovered and put into practice that will produce a significant amount of additional retrievals, in profiles when the reference height is not accessible to the lidar.

We are very pleased, that Reviewer liked our approach

L231-232. Add an earlier reference for spectral dependence of the depolarization ratio, Burton et al. 2015.
Added

L240-241. Since line 223 just said that Veselovskii et al. 2021a already demonstrated that the two dimensional diagram can separate types, is the part about mixtures the main purpose of this manuscript? If so, the abstract and intro should make that clearer and the examples should be chosen to align with that purpose.

We modified Introduction, to show that the main goal is to provide aerosol type mask with high spatio-temporal resolution. The patterns at δ_{532}-G_F diagram help to identify the mixture, but at current stage we can not characterize it quantitatively.

L248-249. Burton et al. (2012) or Burton et al. (2013), referenced elsewhere in the manuscript, is an earlier lidar aerosol classification methodology with depolarization ratio ranges listed for common types.

Added

L247. "The ranges are based on results obtained in LOA". The algorithm is a simple thresholding method in two dimensions, so the ranges are the single most important aspect of the algorithm description. This statement is much too vague to support and explain how the ranges were derived, and I'm eager to know more. What results? From cases published in other publications? From a completely independent subset of cases than the results shown in this manuscript? Are the results only inferences from the lidar measurements of depolarization and fluorescence capacity, or do they include other coincident measurements that provide stronger evidence for the type identifications? Is there a set of training cases that are classified using other external measurements and/or source information? Are the cases shown in this paper the training cases or are they independent cases that demonstrate the validation of the algorithm? All this should be part of the methodology discussion.

We agree with reviewer and completely modified that section. We added:

"**Dust**. The depolarization ratio δ_{532} of Saharan dust near the source regions is up to 35% (Veselovskii et al., 2020a), but after transportation and mixing with local aerosol δ_{532} can be as low as 20% (Rittmeister et al., 2017). In many studies, the dust with decreased depolarization ratio is classified as "polluted dust" (e.g. Burton et al., 2012, 2013). At a moment, we do not introduce the discrimination between the two subtypes and mark as "dust" the particles with 20%<δ_{532}<35%, and $0.1\times10^{-4}<G_F<0.5\times10^{-4}$.

Smoke. In 2021-2022 we regular observed over Lille the smoke layers originated from Californian and Canadian forest fires (Hu et al., 2021). The particle depolarization and fluorescence capacity of transported smoke changed from episode to episode and for classification we choose the ranges 2%<δ_{532}<10%, $2\times10^{-4}<G_F<6\times10^{-4}$. At this stage we do not discriminate "fresh" and "aged" smoke, and the range of δ_{532} variation is similar to the one, used in classification of Burton et al. (2012).

Pollen. The pollen over north of France is usually mixed with other aerosols, and the particles, which we mark as "pollen" are actually the mixtures. Depolarization ratio of clean pollen varies strongly for different taxa. For birch pollen, Cao et al. (2010) reported δ_{532}=33%, and in the measurements over Finland during birch pollination (Bohlmann et al., 2019), observed values of δ_{532} up to 26%. The observations over Lille during pollen season (Veselovskii et al., 2021a) rarely revealed values δ_{532} exceeding 20%. Based on that observations, we type as "pollen" the particles mixtures with 15%<δ_{532}<30%, and $0.8\times10^{-4}<G_F<3.0\times10^{-4}$.

Urban. This type of aerosol includes a variety of particle types (e.g. sulfates, soot) and its parameters may depend on the relative humidity. Based on our measurements inside the boundary layer, for classification we choose the ranges 1%<δ_{532}<8%, and $0.1\times10^{-4}<G_F<0.8\times10^{-}$

[4]. Similar range for δ_{532} is used in classification of Burton et al. (2012). Urban and smoke particles both have a low depolarization, but the fluorescence capacity of smoke is almost one order higher, so these particles can be reliably discriminated.

Ice and water clouds. Both types of the clouds have low fluorescence capacity G_F $<0.01\times10^{-4}$. However, the ice clouds are usually observed at the heights, where fluorescence signal is low and can not be used for classification. Thus above ~8 km the ice cloud are identified by high depolarization ratio $\delta_{532}>40\%$. Depolarization ratio of the liquid water clouds is usually affected by the effects of the multiple scattering, so for their identification we use $\delta_{532}<5\%$."

Figure 3. The mixing lines all go through the box that's marked "pollen". This highlights the unavoidable weakness of typing with just two dimensions. Presumably, anything that falls within this box needs context to distinguish between pollen, a pollen mixture, or a smoke-dust mixture that has nothing to do with pollen. Identification by context (particularly where supporting measurements are available) is fine for the purpose of case studies, but there must be significant potential for misidentification in the automated algorithm, I suppose. It would be good to discuss weaknesses as well as strengths of the approach.

Yes, aerosols are always the mixtures. So this problem is attributed not only to the presented, but also to all existing classification algorithms. Next step in our research is the increase of the number of parameters used and quantifications of mixture components.
It is true, that dust – smoke mixture, considered just at one point at depolarization – fluorescence diagram can be recognized as pollen. This is why it is important to consider all the data obtained during the session. We tried to show in this manuscript that the single pixel data for different mixtures provide different patterns, as shown in Fig.3. In our analysis we always observed this kind of patterns, and it helps to get idea about mixture composition.

L268. Clouds are also shown in the aerosol typing masks and line 308 mentions both ice and water droplets, so the thresholds values for ice and water droplets should also be included in Table 1.
Figs 4,5. It's confusing that the ice cloud is only partially included in this example. It's shown in the type mask, but not discussed, and it's not shown in the scatter plot in Fig 5a. It's included in Fig 4, but apparently off-scale. The authors should decide whether they want to include the cloud in their analysis and discussion or not. If not, cut off the plots at an altitude below the cloud. If so, rescale Figure 4, include it in Fig 5 and add discussion about cloud.

The parameters for ice and water particles are added to the Table 1. The ice clouds, however, are normally observed at high altitudes, where fluorescence signal is very weak, so corresponding points at depolarization – fluorescence diagram demonstrate strong scattering. Usually we identified the ice crystals from depolarization measurements only, and this is why we don't show them in Fig.5a. Corresponding comment is added to the revised manuscript.

Figure 5 and similar figures. What's the purpose of the boxes and cross-hairs in the fluorescence vs. depolarization diagrams? The boxes would probably be more useful to readers if they were all the same, and used the values from Table 1. That way, we can see visually how the identified types fall into the broad category already established. I can guess that the crosshairs represent the mean and (probably) standard deviation of identified pure types, but those aren't discussed anywhere in the paper.

In our revised manuscript the boxes correspond to Table 1. The crosses show uncertainty of our measurements, due to statistical errors and uncertainty of calibration. Corresponding comment is added to revised manuscript.

L315-321. The explanation of the smoothing procedure is missing something. Z is a number, but the classification IDs are not numbers that can be added and weighted, but just labels. How are the classifications convolved with Z? Just guessing, I suppose the fluorescence capacity and depolarization ratio are what's averaged using the Z-weightings, and then the classification is done on these smoothed measurements instead? Please clarify in the text.

To make it more clear, we modified corresponding section in the revised manuscript and extended description.
Briefly:
We construct several 'raw' matrices with dimensions equal to primary data matrices (one matrix for each aerosol type (dust, pollen, etc)). If at the first stage some single pixel data point (i,j) is classified as, e.g., pollen, the corresponding value in the 'pollen' matrix is set to 1, otherwise it is set to 0. Then each of these matrices is separately convoluted with the Gauss kernel Z. And, after the convolution, the values for each pixel data (i,j) are being compared. If, e.g., the 'dust' matrix (after the convolution) contains maximal value at the point (i,j) among all the matrices (after the convolution), then the point (i,j) is finally classified as 'dust'.

L339 and 341 and elsewhere. I'd suggest avoiding describing values as "typical" and expand the description to be more specific. For instance, perhaps this is within the ranges seen in your previous publications and/or other publications for cases that have been identified as smoke and urban based on independent data? "Typical" is a bit dangerous, in that it implies a generality that is not established after only a few handfuls of case studies, particularly since the case study identifications seem to mostly be rather dependent on expectations about the typical values. Statements like this unfortunately seem to be quoted and referenced repeatedly so that they become ingrained without becoming better supported. After all, we now know that it is quite common for smoke (in the upper troposphere and stratosphere) to have depolarization values that are much larger than this, and previously published ranges of depolarization for urban aerosol also include significantly larger depolarization values than this.

Agree. We tried to follow this recommendation in revised manuscript
It is true, that aged smoke depolarization ratio at 532 nm in stratosphere can be as high as ~20%. We should mention also, that at 1064 nm the depolarization ratio of smoke in our measurements (even in upper troposphere) never exceeded 5%. This is one more reason to include this depolarization ratio in typing scheme at next stage.

L347. Says that the fluorescence capacity can decrease as a function of relative humidity, explaining a range of variables. Why does it produce variability rather than reducing the fluorescence capacity uniformly?

The water uptake increases the particle backscattering, but does not change the fluorescence. As a result, the fluorescence capacity decreases. The RH, changes with height, which can lead to increase of single pixel data scattering inside the cluster.

L361-367 and Figure 6-7. I agree that the shape of the curve in Figure 7a is very striking and reminiscent of a mixing line. However, I also just read in the previous section that fluorescence capacity is strongly impacted by relative humidity, making me wonder quantitatively how much impact RH has, compared to the impact of mixing. Is there a model (theoretical or empirical) of G_F dependence on relative humidity? The RH profile should be added to Figure 8 (and all the other profile figures). Another aspect that puzzles *and surprises me is the increased G_F specifically in parts of the curtain where the backscatter is lower. This hints that the variation in G_F might be quite strongly related to RH; alternately that the pollen is more diffuse and widespread than the urban aerosol, which I think would be unusual. A curtain of RH (perhaps from MERRA-2 since there is insufficient sonde data to produce a curtain) and/or backtrajectories might help make the scenario more clear.*

Unfortunately, we had no collocated RH measurements. The sonde measurements in UK show that RH increased from 40% to 70% with height. The value of the fluorescence capacity changed for one order of magnitude, and such strong change in G_F can not be explained by the particle hygroscopic growth. For example, from the recent publication of Sicard et al., increase of β_{532} in this RH range for urban aerosol is below factor 1.5. (Sicard, M., Fortunato dos Santos Oliveira, D. C., Muñoz-Porcar, C., Gil-Díaz, C., Comerón, A., Rodríguez-Gómez, A., and Dios Otín, F.: Measurement Report: Spectral and statistical analysis of aerosol hygroscopic growth from multi-wavelength lidar measurements in Barcelona, Spain, Atmos. Chem. Phys. 22, 7681–7697, 2022). Corresponding comment is added to revised manuscript.

The hygroscopic growth can contribute to the backscattering near the PBL top. However, at low altitudes RH is about 40%, so increase of G_F is probably due to decrease of urban particles contribution to the total backscattering (thus pollen contribution becomes more visible).
We tried to use MERRA-2 data, but at low altitudes the modeled parameters differed strongly from observations.

L368-369. It's good that 1064 nm depolarization is included here, because in general, the more data shown, the better the patterns can be understood. However, the text highlights larger values of 1064 nm depolarization to support the inference of pollen, but that's also true for urban aerosol (e.g. Burton et al. 2012). Then "both depolarization ratios decrease with height" as the pollen concentration decreases (L372), but 1064 continues to be larger than 532, so again this is not definitive. Any further comment about this?

Yes, urban aerosol may also have δ_{1064} exceeding δ_{532}. But absolute values of depolarization for pollen are significantly higher. So when at low altitudes we observe high G_F, and high depolarization, the observed $\delta_{1064} > \delta_{532}$ corroborates presence of pollen.

This case and the first case were also included in earlier publications by the same authors. The papers make different analyses of them, so that's fine, but does this mean they also contributed information relevant to producing the ranges used in the algorithm? If so, they are not such good examples to illustrate the performance of the typing algorithm.

The typing is performed on a base of G_F-δ_{532} measurements only. We used these examples, because the aerosol origin was analyzed in our previous publications. Besides, measurements on 30 May 2020 demonstrate very characteristic pattern for urban – pollen mixture.

The vertical profiles of particle parameters for 30 May were presented in our recent paper, so we decided to exclude Fig.8 from revised manuscript. We just provide the reference.

Figure 8 L 715. Why were the profiles created for 21:00-23:00 instead of a later time where the curtain shows pollen at lower altitudes and mixing is discussed? Is this a mistake?

Sorry, this was mistake.

L376-377. I'm not finding the explanation for the lack of variability in the backscatter angstrom exponent to be very convincing. It appears to be saying that the urban particles are growing due to humidification exactly in balance with the effective dry particle size decreasing due to less pollen? (if so, this needs support).
Perhaps some quantitative modeling would help. How small of a backscatter Angstrom exponent would be expected for high concentration of pollen, and just how much contribution to the backscatter is there (based on the mixing model) and how much change in Angstrom would you therefore expect? What confuses me is that the fluorescence capacity also mixes linearly according to the backscatter partition, so if there was really too little backscatter contribution to be noticeable, wouldn't that also mean there would be little variation in G_F as well?

In revised manuscript, this section was completely modified. We agree with reviewer, that behavior of backscatter Angstrom 532/1064 is puzzling. However, the observation presented, could be strongly influenced by hygroscopic growth, which decreases both depolarization and the fluorescence capacity. The backscattering Angstrom exponent strongly (and in complicated way) depends on refractive index, particle size and particle shape. The modeling of the BAE for different mixture compositions is important, but it is out of scope of this research. Just want to mention, that that in publication of Bohlmann et al. (2019) the BAE (at depolarization ratio ~20%) is about 1.0. Which is quite high value and pollen content over Finland is significantly higher than over Lille. So this aspect needs additional research and additional measurements during strong pollen episodes.

L392-393. Unfortunately, the SILAM website only provides current forecast data, so please make the relevant data available as a supplement or shown in a figure. Also, what kind of pollen was it?

In situ measurements at the roof of the building demonstrate presence of significant amount of grass pollen. We added to the revised manuscript (as Appendix) the SILAM maps for four episodes, when presence of pollen was assumed.

L418-419. I'm not quite clear on what the author's intent is here. Is this saying that the algorithm misclassified a mixture as pure urban, or that the mixture only occurs where the classification puts it, but that the two urban layers have quite a lot of difference between them? It would be very helpful (in this case and others) to mark the points in the scatterplots according to the classification result or altitude. I would like to see exactly where the two layers classified as "urban" fall on the apparent mixing line. I think it's interesting that the two layers marked urban have different spectral dependence of depolarization. Backtrajectories would be helpful for this case too, to help understand why the two layers of urban aerosol might have different properties.

To make presentation more clear, we significantly modified this section. First of all, in depolarization – fluorescence diagram in Fig.12 we show the points related to the upper and lower layers by different colors. Back trajectories analysis shows that air masses in both layers are transported from England. So this is probably pollution. Points related to the upper layer are inside the range for ‘urban” aerosol. Points in the lower layer, are partly outside of this range, so the aerosol type is undefined. We assume that this is the mixture of urban and pollen particles, because we have particles with high depolarization and fluorescence capacity (still not high enough to be classified as “pollen”). This mixture is marked by grey color and it is located below 750 m. The maps with SILAM pollen index are added to the revised manuscript as Appendix. On the midnight of 10-11 April 2020 the pollen loading is modeled by SILAM as moderate.
Thus yes, properties of layers are different. Upper layer is urban, while in lower layer below 1 km the urban particles are mixed with pollen.

L420. "typical for urban-pollen mixture". Actually the mixing curve is significantly to the left of the curve in Figure 3, suggesting that the pure pollen in this mixture is not "typical" compared to the ranges given in the table, but is more of an edge case with relatively low fluorescence capacity.

Yes, fluorescence capacity is lower than usual, so this not pure pollen. We added corresponding comment to the text.

L430-436. This is a very nice case to demonstrate contrast in fluorescence between different types. But the type identification is entirely made by inference using the two classification dimensions without any other support such as in situ measurements, backtrajectories, or other lidar-measured quantities like 1064 nm depolarization, lidar ratio or angstrom exponents. It's great that two measurements used for the classification appear to give the ability to make these separations, but for such a key demonstration I think the case studies need to be very well supported. In general I suggest bolstering the verification of the identifications for all the cases (not just this one) by including all relevant data. I mean specifically, first of all, other lidar quantities that have been used in previous classification methodologies, including especially lidar ratios, and also 1064 nm depolarization and angstrom exponents for all cases. Also include RH, backtrajectories and any coincident in situ measurements (especially pollen) for all cases.

In the revised manuscript we added the Table 2, with main intensive particle parameters for all episode considered. The section is modified: we added backtrajectories and analysis of the intensive particle parameters. We have added also Table 3, which compares our observed intensive parameters for dust, smoke, urban with parameters used in existing typing algorithms.

L445 and Figs 15 and 16. The suggested mixing between layers doesn't look convincing. On the fluorescence vs. depolarization diagram, these intermediate points don't follow a nice mixing line like the other mixing cases, and the boundaries in the measurement curtains appear quite crisp. Could these points be artifacts of the smoothing instead?

Yes, at high gradients of backscattering, smoothing sometimes can provide oscillation. We reprocessed this case with decreased smoothing. The threshold value of β_{532} was increased up to 0.3 Mm-1sr-1. Now it is better.

Fig 15. The depolarization especially and perhaps also the fluorescence capacity (outside of the smoke plume) seems to be anti-correlated with backscatter, including in regions that seem unlikely to be pollen-dominated (such as the minimum between the smoke and urban layers). Particulate depolarization is especially susceptible to systematic error, particularly overestimation, at low values of backscatter (Freudenthaler et al. 2009, Burton et al. 2015). Have you done a systematic uncertainty calculation? (Also this is another case where color coding of the scatterplot by altitude would be useful).

Yes, calculation of depolarization at low β_{532} can lead to enhanced uncertainty, especially when high gradients of β_{532} present. In reprocessed data we increased threshold value of β_{532} up to 0.3 Mm-1sr-1. Oscillations decreased. The same is true for fluorescence capacity.
We estimate uncertainty of our depolarization calibration to be below 15%.

Fig 15-18. Include the data for depolarization and angstrom exponent (and RH) for these cases also.

In the revised manuscript we have added Figures 16, 19 with vertical profiles for these episodes.

L455 "G_F increased ... probably due to the mixing with local pollution". Does this make sense? Nothing prior to this in the manuscript suggests that urban pollution has significant fluorescence capacity. Also, on the scatter plot on Figure 18, there's no suggestion that the higher values of G_F in the dust cluster are correlated with depolarization in any way; that is, they are not following any mixing line. What evidence is there that this is not simply normal variability within dust? Table 1 shows dust can have G_F up to 0.5. Why not 0.6? Also, could some of this variability be correlated with RH?

Dust may have very low fluorescence capacity (0.1*10^-4), while urban particles for some episodes had G_F of 0.8*10^-4, or even higher. Thus mixing of dust with pollutions, in principle, can increase the capacity. But reviewer is right, for case presented, the depolarization ratio did not change significantly with height, while capacity strongly decreased in the center of the layer. It can be variation of dust composition (and so the absorption) through the layer. Unfortunately, at this stage we can not make definite conclusion. Corresponding section is strongly modified in revised manuscript.

For the available dust episodes the fluorescence capacity was mainly below 0.5*10^-4. This is why we used it in Table 1. We may reconsider this range, when more data will be available.

Normally properties of dust are not very sensitive to RH. Increase of RH can only decrease the capacity. However at a moment we don't have collocated RH measurements, so unable to make quantitative conclusions about RH influence.

L485. "during Spring-Autumn seasons". It would be helpful to show a timeseries demonstrating that the pollen signature (elevated depolarization and fluorescence capacity) does NOT occur in winter.

We agree, that this would be useful, but it is beyond the scope of this manuscript. Seasonal variation of aerosol composition over Lille will be the topic of separate research.

Typographical or wording:
L19. What is meant by "single" in "first single version of the algorithm". I suggest delete "single" or reword.
Corrected

L18 and L24. Change particle's to particle.
Corrected

L92. Be specific about which wavelength here.
Done

L247. Define LOA.
Done

L270-281. There should be some discussion or at least references to other analyses of mixtures of aerosols that derive similar equations (especially Eq. 7), e.g. Sugimoto and Lee 2006, Gross et al. 2011, Gasteiger et al. 2011, Tesche et al. 2009, Burton et al. 2014.

The references are added. Derivation of Eq.7 looks very straightforward, so probably no explanations are needed.

L280. Eq. 8. It probably would be good to remind the reader that fluorescence capacity and backscatter in this equation refer to particular wavelengths.
Done

L282. "We assume". I think this is meant to refer only to the demonstration in Figure 3, not a general assertion. If true, perhaps swap the first two sentences of the paragraph to make it less likely to be misread. As mentioned in the introduction, the quantities have a lot of variability even within types, so assuming single values wouldn't be well supported.

Done

L300. "the height resolution is 7.5 m". Is that really the resolution or only the grid spacing? That is, taking the detectors into account, are measurements at adjacent vertical grid points independent?

Yes, this is bin resolution of our detection electronics, and in many cases this resolution was used to calculate the particle properties. However, for elevated layers the fluorescence signal was splined. For typing, the Gaussian smoothing procedure was used. Thus ultimate resolution was about 60 m for height and less than 10 minutes for time.

L342. spell out FBC
The section was modified

L344. Add a reference to the reminder. (I think it is Veselovskii 2020?)
Done

L445. Typo in "0.2-0.3"
Corrected

L663-664. It would be helpful to add "using the reference height as Ansmann et al. 1992 (green) or the calibration constant as in Eq 5. (magenta)". (I read figure captions before the text, so having a bit more detail in the captions is very helpful)
Done

L708. Please add clarification to the caption whether the scatter plot shows data for the entire time period shown in the curtain or only the subset that's included in the profile plots of Figure 8.
This is for entire time period. Added to caption.

Figure 2 and 4. There is a lot of red in these plots hinting that the scales might be cutting off the data. Perhaps the scales should be expanded.
Yes, this is because depolarization and backscattering of clouds is very high, comparing to aerosol. We choose such scale, to make details of aerosol more visible. So we would prefer to keep as it is.

Figure 3. Also show the smoke + pollen mixing line, since one of the selected cases references mixing of those two types.
We though to do it, but figure becomes overloaded with curves. Beside, behavior of this mixing line is quite obvious, so we think that it is not so necessary for reader.

Figures 4, 6, 912, 15, 17. It would be helpful if the curtains of intensive properties (depolarization and fluorescence capacity) had consistent scales across each of these plots, making it easier to compare one case to another.
Unfortunately, the cases are very different. In some elevated layers are considered, and in some only the PBL. So we used different scales to show the details. We would prefer to keep different scales for each episode.

References:
Burton, S. P., et al. (2014) Separating mixtures of aerosol types in airborne High Spectral Resolution Lidar data. Atmos. Meas. Tech. 7, 419-436 DOI: 10.5194/amt-7-419-2014
Burton, S. P., et al. (2015) Observations of the spectral dependence of linear particle depolarization ratio of aerosols using NASA Langley airborne High Spectral Resolution Lidar. Atmos. Chem. Phys. 15, 13453-13473 DOI: 10.5194/acp-15-13453-2015

Freudenthaler, V., et al. (2009) Depolarization ratio profiling at several wavelengths in pure Saharan dust during SAMUM 2006. Tellus B 61, 165-179 DOI: 10.1111/j.1600-0889.2008.00396.x
Gasteiger, J. and V. Freudenthaler (2014) Benefit of depolarization ratio at λ = 1064 nm for the retrieval of the aerosol microphysics from lidar measurements. Atmos. Meas. Tech. 7, 3773-3781 DOI: 10.5194/amt-7-3773-2014
Groß, S., et al. (2011) Characterization of Saharan dust, marine aerosols and mixtures of biomass-burning aerosols and dust by means of multi-wavelength depolarization and Raman lidar measurements during SAMUM 2. Tellus B 63, 706-724 DOI: 10.1111/j.1600-0889.2011.00556.x
Sugimoto, N. and C. H. Lee (2006) Characteristics of dust aerosols inferred from lidar depolarization measurements at two wavelengths. Applied Optics 45, 7468-7474 DOI: 10.1364/AO.45.007468
Tesche, M., et al. (2009). "Vertically resolved separation of dust and smoke over Cape Verde using multiwavelength Raman and polarization lidars during Saharan Mineral Dust Experiment 2008." J. Geophys. Res. 114(D13): D13202.

References are added